Engineering zeolite pellets for the adsorption of organic micropollutants

A.A. Elshof

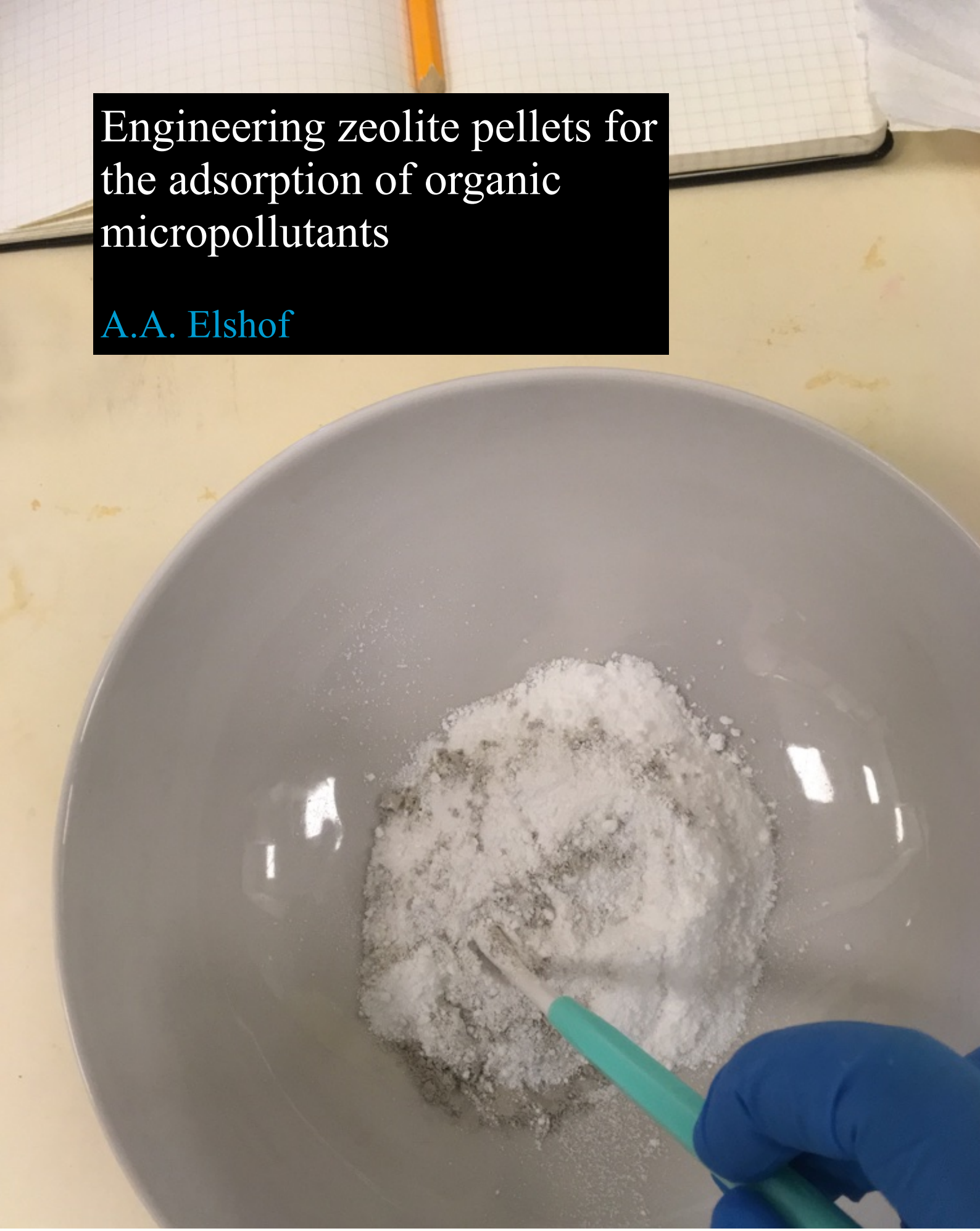

TU Delft Delft University of Technology

Challenge the future

Engineering of zeolite pellets for the adsorption of organic micropollutants

by

Andrea Anna Elshof

for the degree of
Master of Science in Civil Engineering
12 June 2019

Assessment Committee

Prof.dr.ir. L.C. Rietveld	TU Delft, Sanitary Engineering
Dr.ir. S.G.J. Heijman	TU Delft, Sanitary Engineering
Dr.ir. G.M.H. Meesters	TU Delft, Product and Process Engineering

Department of Sanitary Engineering
Faculty of Civil Engineering and Geosciences
Delft University of Technology

TU Delft Delft University of Technology

Abstract

Our use of pharmaceuticals, pesticides and personal care products leads to an increase of organic micropollutants (OMPs) into the aquatic environment. Conventional wastewater treatment plants are not designed for the removal of OMPs and need to be upgraded to reduce OMP contamination. The adsorption of OMPs to zeolites is proposed as an alternative treatment method. Zeolites are synthesized as powders, however they need to be shaped into pellets to be used in water treatment practice. This research focussed on engineering zeolite pellets and which properties of these pellets are important for the adsorption of OMPs.

First the influence of the calcination temperature and binder content on the mechanical stability and porosity of the pellets was analysed. Second, the influence of two different preparation techniques (extrusion and high-shear granulation) and the introduction of a polymer on the mechanical stability, porosity and adsorption kinetics of the pellets was assessed. Third, the effect of the porosity on the breakthrough for an empty bed contact time (EBCT) of 20, 5 and 1 minute(s) was determined according to the linear driving force (LDF) model.

It was found that an increasing binder content and calcination temperature increased the wear resistance and porosity of the pellets. However, the effect on the porosity is minimal. The introduction of the polymer had opposite effect on extruded and granulated pellets. For extruded pellets, the introduction of the polymer increased the porosity. However, the granulated pellets showed a decrease in porosity. A relation was found between the porosity and the wear resistance and between the porosity and adsorption kinetics. A larger porosity decreased the wear resistance of the pellets and increased the kinetic rate constant.

The porosity was of great importance in relation to the breakthrough. First, the porosity in the zeolite pellets determined to a great extent the bulk density of the filter bed. A higher bulk density resulted in a later breakthrough point. The bulk density was also influenced by the shape of the pellet. Spherically-shaped (granulated) pellets had a higher bulk density than rod-shaped (extruded) pellets. Second, the porosity was related to the kinetic rate constant. At lower EBCTs (5 and 1 minute), the kinetic rate constant had an influence on the breakthrough point. For these EBCTs, a higher kinetic rate constant led to a later breakthrough point.

It was recommended to optimize the zeolite pellets by making the extruded pellets in a more spherically-shaped form and to start column experiments to validate the LDF-model.

Contents

List of Abbreviations

BOM	Background organic matter
EBCT	Empty bed contact time
LDF	Linear driving force
MIP	Mercury intrusion porosimetry
OMP	Organic micropollutants
WWTP	Wastewater treatment plant

Chapter 1

Introduction

1.1 Organic micropollutants

Organic micropollutants (OMPs) are compounds, which are used every day in modern society, including pharmaceuticals, synthetically and naturally occurring hormones, pesticides and personal care products. OMPs occur in very low concentrations in the aquatic environment, in the order of ng/L to μg/L. Over the last decades, the awareness of the impact of OMPs has grown and due to improved analytical techniques more OMPs are detected in both surface and drinking water (STOWA, 2014).

OMPs enter the aquatic environment in several ways. A simplified version of the main sources and pathways of OMPs into the environment are shown in Figure 1.1. Pesticides are washed away from agricultural areas into surface water and groundwater. Personal care products end up in the wastewater during showering or washing hands. Pharmaceuticals and hormones are excreted via urine and faeces. A major source is wastewater of households, industry and hospitals (Tijani et al., 2013; Yunlong et al., 2014). Wastewater is collected using a sewer and transported to a wastewater treatment plant (WWTP) to be treated. Conventional WWTPs are designed to remove organic substances, nitrogen and phosphate, whereas OMPs are only partially removed (Grontmij, 2011; Liu et al., 2009; Petrovi et al., 2003; Yunlong et al., 2014). In particular the non-biodegradable OMPs are hardly removed, such as antibiotics and the widely used pharmaceutical diclofenac (Grontmij, 2011; Yunlong et al., 2014). Due to the low removal efficiency for OMPs, the remaining OMPs are discharged to receiving water bodies and thus introduced into the environment.

Drinking water companies extract surface water and groundwater for the production of drinking water. During the treatment process of drinking water OMPs are removed in a wide range of efficiency by granular activated carbon filtration (Stackelberg et al., 2007). OMPs, even though in low concentrations, are still present in drinking water and have even been detected in human blood and urine (Hutter et al., 2005; Kannan et al., 2005; Stackelberg et al., 2007). Due to the low concentrations of OMPs in drinking water the expected risk to public health is low, however the long-term effects are still unknown (de Jesus Gaffney et al., 2015; Schwab et al., 2005; Schwarzenbach et al., 2006).

The aquatic life is affected by OMPs present in the environment (Adeel et al., 2017; Bolong et al., 2009; Crane et al., 2006). The best known example is the feminization of male fish due to the presence of estrogenic substances in water (Kidd et al., 2007; Tetreault et al., 2011; Vethaak et al., 2002). Stopping the inflow of OMPs into the aquatic environment is an

ongoing challenge for the water authorities.

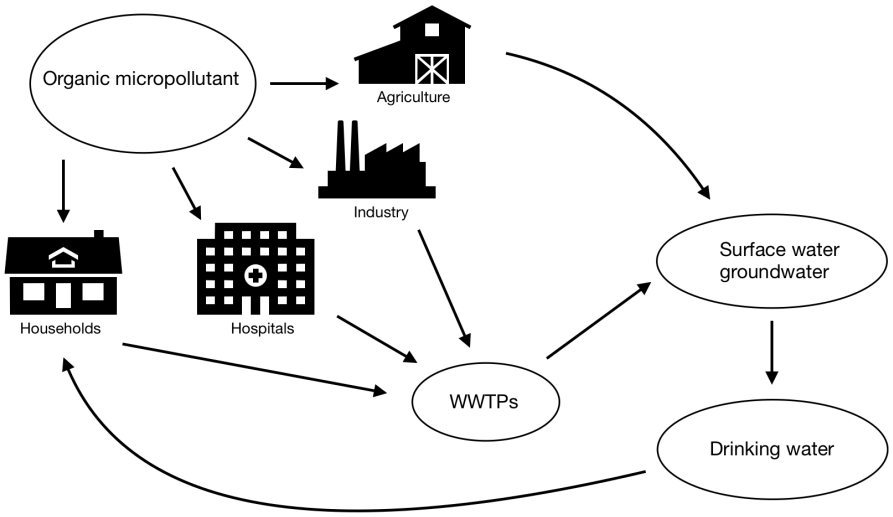

Figure 1.1: Sources and pathways of OMPs into the environment

1.2 Treatment options for the removal of OMPs from domestic wastewater

Over the years, different treatment options to remove OMPs from domestic wastewater have been investigated, of which adsorption by activated carbon is one of the most effective treatment steps for OMP removal (Bolong et al., 2009; Rivera-Utrilla et al., 2013; Stackelberg et al., 2007; Tijani et al., 2013). The pore structure and large surface area enables the activated carbon to adsorb a broad spectrum of OMPs (Rossner et al., 2009). To restore the adsorption capacity, the saturated activated carbon is regenerated and can be reused. However, the production and thermal regeneration of activated carbon is costly and has a negative impact on the environment (Arena et al., 2016; Mousel et al., 2017). Regeneration also results in a loss of carbon (4-8%) (Tchobanoglous et al., 2003), meaning that new carbon needs to be purchased. Furthermore, due to a large amount of background organic matter (BOM) in wastewater, the OMPs experience competition for the adsorption on activated carbon. The presence of BOM results in a faster saturation of activated carbon (Hu et al., 2015; Zietzschmann et al., 2016). Therefore, the activated carbon needs to be regenerated more often.

The challenge is to implement a low cost wastewater technology with low environmental impact and high OMP-removal efficiencies. Together with Applied and Engineering Sciences (TTW), Foundation for Applied Water Research (STOWA), TKI Watertechnology and KWR, the Delft University of Technology will investigate an innovative adsorption-oxidation process (AdOx). This proposed process consists of a combination of several removal processes, including the adsorption of OMPs to zeolites and the regeneration of saturated zeolites using ozone. This research focused on the adsorption of OMPs to zeolites.

1.3 Adsorption

Adsorption is a surface-based process in which atoms, ions or molecules adhere to a surface, see Figure 1.2. The adsorbing material is called the adsorbent and the substance being adsorbed is the adsorbate.

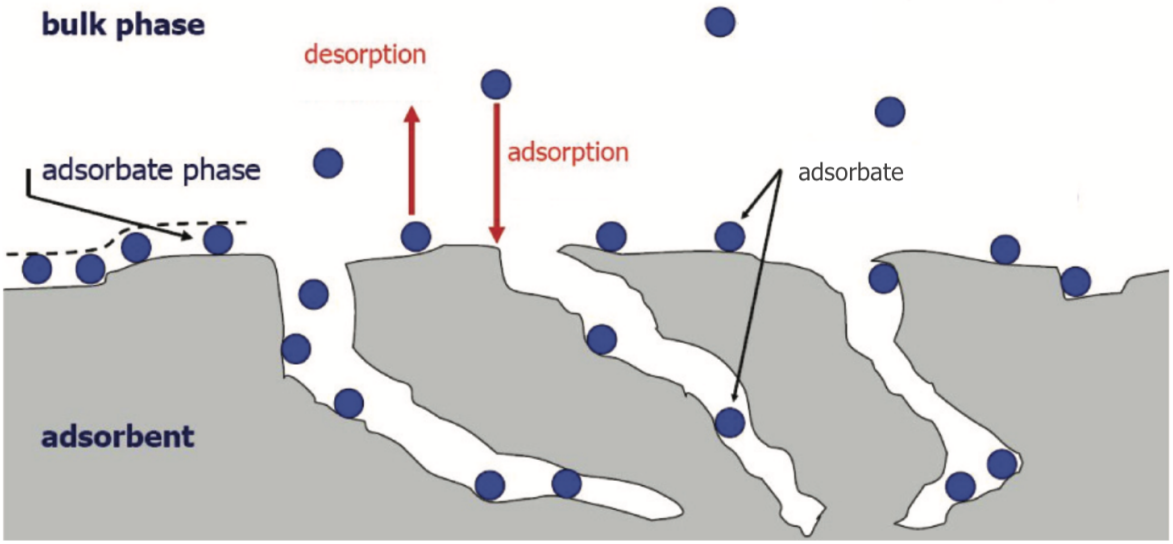

Figure 1.2: Schematic overview of adsorption process

Adsorption is a dynamic process, where the adsorbate adsorbs onto and desorbs from the adsorbent. The adsorption process is in equilibrium when the rate of adsorption is equal to the rate of desorption. This equilibrium depends on the adsorbate concentration and the water temperature. The relation between the amount of adsorbate adsorbed on the surface of the adsorbent and the concentration of the adsorbate at constant temperature can be described by an adsorption isotherm. The Freundlich isotherm is often used to describe this relation for low adsorbate concentrations (Equation 1.1).

$$q_e = K_F C_e^n \tag{1.1}$$

where

q_e = the amount of adsorbate per mass unit of adsorbent at equilibrium $[mg/g]$
C_e = the liquid-phase concentration of the adsorbate at equilibrium $[mg/L]$
K_F = the Freundlich capacity factor $[(mg/g)(L/mg)^n]$
n = the Freundlich intensity parameter $[-]$

Adsorption (by activated carbon) is a widely used water treatment step. Fixed bed reactors are filled with the adsorbing material and exposed to high water flows. During this process the filter bed gets saturated over time (Figure 1.3). The moment the adsorbate concentration in the effluent exceeds a set threshold (c_b) is known as breakthrough. The filter then needs to be renewed or regenerated before the process repeats itself.

Before actual fixed bed reactors are designed, the operational variables and design parameters are established from laboratory-scale column experiments and predictions from math-

ematical models, such as the linear driving force (LDF) model (Heijman et al., 2002; Sharma et al., 2003).

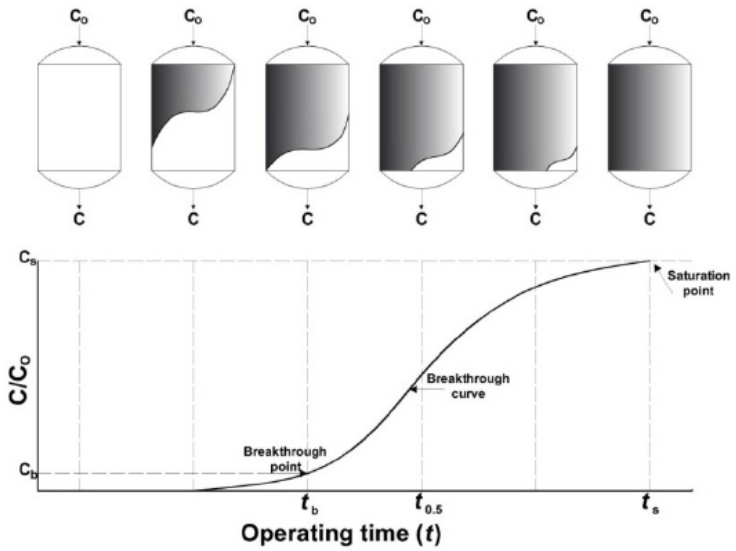

Figure 1.3: Schematic of a breakthrough curve in a fixed bed adsorption process

1.4 Zeolites

Zeolites are porous crystalline materials constructed from SiO_4 and AlO_4 tetrahedrons. They have a 3-dimensional microporous structure containing uniformly distributed channels and cavities with pore sizes less than 1 nm (Ruthven, 1984). Zeolites are widely used as catalysts in the petrochemical industry, as ion exchanger in water softening devices such as laundry detergents and as molecular sieves for gas separation. In recent years, zeolites have also been found to be effective adsorbents for the removal of OMPs (Abu-Lail et al., 2010; Yonli et al., 2012).

Up to now, 235 different zeolite framework structures have been identified by the Structure Commission of the International Zeolite Association (Baerlocher et al., 2007). Each framework type stands for a unique structure of channels and cavities. Four framework types (FAU, MOR, MFI and BEA) are found to be most effective for the adsorption of OMPs (Jiang et al., 2018).

The microporous uniform structure enables the zeolites to selectively sort molecules based on size. The molecular sizes of most OMPs are similar to the pore size of zeolites. Therefore zeolites are able to adsorb OMPs without competition of BOM (Abu-Lail et al., 2010; Tchobanoglous et al., 2003). Although, BOM can still block the pores and thus decrease the adsorption kinetics of OMPs (Hung and Lin, 2006). Furthermore, it is assumed that closely fitted pores lead to strong interactions between OMPs and zeolites (Tchobanoglous et al., 2003). The alumina content determines the hydrophobicity of the zeolites. High-silica zeolites with Si/Al ratios from 5 or more have hydrophobic surfaces (Ruthven, 1984; Yonli et al., 2012). The hydrophobic surface prevents the zeolites from adsorbing water, which

means that more pores are available for OMP diffusion and adsorption (Tchobanoglous et al., 2003). Another feature of zeolites is its chemical stability. This gives the zeolite potential to be regenerated by oxidation, like ozone, without changing the surface properties and pore structure (Zhang et al., 2014).

Zeolites are synthesized as polycrystalline powders with a particle size of 1-10 μm (Ruthven, 1984). However, in order to use zeolites as adsorbents in water treatment practice the powdered zeolites need to be shaped into macroscopic forms, like granules, extrudates or pellets to avoid high pressure drops in the reactor. Pure powdered zeolites do not possess binding abilities. An inorganic binder, mostly natural clays, are mixed with zeolite powder in a range of 10 wt.% to 30 wt.% and water to form pellets (Jasra et al., 2003; Ruthven, 1984). The pellets are calcined to ensure mechanically stable particles. The high-temperature treatment destroys the surface area and activity of the clay (Jasra et al., 2003).

Extrusion and high-shear granulation are two processes to create pellets. Extrusion is a process where the mixture is pushed through a die with a specific cross-section. In high-shear granulation, the powder and water are mixed in a bowl by a rotating impeller. As the water disperses throughout the powder, granules are formed. The advantages of extrusion are a higher yield and wear resistance (Keleb et al., 2004).

During the shaping process a secondary pore system is created (Figure 1.4) consisting of mesopores (2-50 nm) and macropores (>50 nm) within which the adsorbate has to move to the zeolite crystals (Jasra et al., 2003). The secondary pore system is important because it may cause transport limitations. Pellets with a more open secondary pore system, so a larger amount of macropores, show faster adsorption kinetics (Schumann et al., 2012).

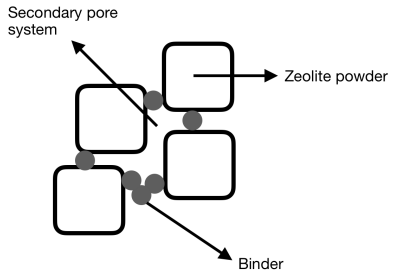

Figure 1.4: Schematic view of secondary pore system (not on scale)

In order to increase the secondary pore system, polymers can be added to the zeolite-binder mixture (Mueller et al., 2006; Sextl et al., 1994). Polymer is mixed with water and after a certain maturation time, the polymer chains unfold to their full capacity. When the polymer solution is added to the zeolite-binder mixture, the polymer chains create a larger secondary pore system (Figure 1.5).

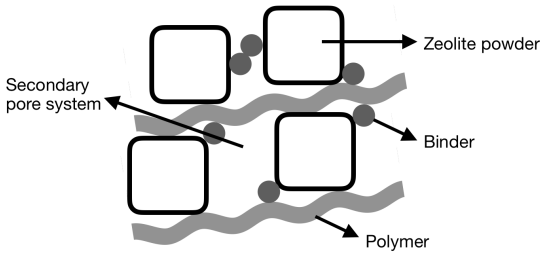

Figure 1.5: Schematic view of secondary pore system with polymer (not on scale)

1.5 Knowledge gap and objectives

Even though zeolite pellets are already used for several applications, they have not been fabricated to be used in WWTPs. The research in the water treatment field has mainly been focused on whether zeolites could be an alternative for the adsorption of OMPs. However, in all these studies the zeolites are examined in powder form. This presented research focussed on engineering zeolite pellets and which properties of these pellets are important for the adsorption of OMPs.

The first step in engineering zeolite pellets was to determine whether temperature and binder content influence the mechanical stability and porosity of the pellets. Second, we compared two different preparation techniques and assessed whether the introduction of a polymer influences the mechanical stability, porosity and adsorption kinetics of the pellets. Third, we aimed to determine which property of the zeolite pellet has the most effect on the breakthrough.

The main research question was:

What are important properties of a zeolite pellet to achieve efficient OMP adsorption?

The sub-questions were:

- What is the effect of the binder content and calcination temperature on the wear resistance?
- What is the effect of the binder content and calcination temperature on the pore size distribution?
- What is the effect of introducing a polymer in zeolite pellets?
- What is the effect of increasing the porosity in zeolite pellets on the predicted breakthrough according to the LDF model?

Chapter 2

Materials and methods

2.1 Research overview

In this research pellets with different configurations and preparation techniques were engineered. First, both the binder content and calcination temperature were altered to analyse its effect on the strength and porosity. Second, a polymer was added to the mixture to increase the secondary pore system. This was done for two different preparation techniques; extrusion and high-shear granulation. Third, the breakthrough curves of the pellets were simulated.

2.1.1 Engineering of zeolite pellets

In the first stage of this thesis, the effect of the binder content and calcination temperature on the wear resistance and pore size distribution of the pellets were determined.

Pellets with three different binder percentages were prepared. These pellets were calcined at three different temperatures, resulting in nine pellets (Table 2.1). The preparation technique used in this phase was extrusion.

Table 2.1: Nine different pellet configurations

Binder content [%] \ Temperature [°C]	750	850	950
15	X	X	X
20	X	X	X
25	X	X	X

The pellets were subjected to wear resistance and porosity tests. Table 2.2 shows which tests have been conducted per pellet. Based on the results from the strength and porosity tests, the pellet with a binder content of 15% and calcination temperature of 750°C was chosen to be used in the continuation of this research.

2.1.2 Introduction of polymer to zeolite pellets

The pellet configuration of 15% and 750°C was used to both prepare extruded as granulated pellets. In both the extruded as the granulated pellets a polymer was introduced to increase the porosity. In total, four different pellet configurations were used, Table 2.3.

Table 2.2: Tests conducted with the nine different pellets

Binder content [%]	15			20			25		
Temperature [°C]	750	850	950	750	850	950	750	850	950
Wear resistance	X	X	X	X	X	X	X	X	X
Porosity	X	X	X	X			X		

Again, both the wear resistance and porosity was tested. In addition, methylene blue adsorption experiments were conducted to determine the LDF kinetic rate constant.

To check for reproducibility, the two extruded pellets were made in duplicate and the results were compared.

Table 2.3: Four different pellet configurations

	Polymer	
	No	Yes
Extruded	X	X
Granulated	X	X

2.1.3 Modelling of breakthrough

In the last stage, the results from the adsorption experiments, the LDF kinetic rate constant, was used to simulate the breakthrough curve. The influence of the LDF kinetic rate constant and the properties of the pellets was analysed.

2.1.4 Overview zeolite pellets

In total, 12 different pellets were made, tested and analysed. In addition, two pellets were made in duplicate. The engineered zeolite pellets are summarised in Table 2.4. The code name of the zeolite pellets is explained in Figure 2.1.

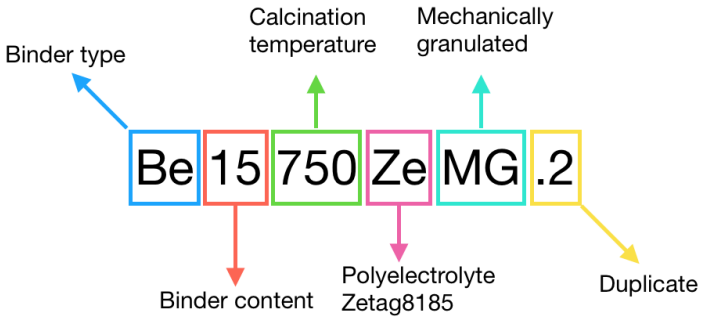

Figure 2.1: Explanation of the code name of the zeolite pellets

Table 2.4: Overview of engineered zeolite pellets

Code name	Binder content [%]	Temperature [°C]	Polymer
Be15750	15	750	-
Be15750.2	15	750	-
Be15850	15	850	-
Be15950	15	950	-
Be20750	20	750	-
Be20850	20	850	-
Be20950	20	950	-
Be25750	25	750	-
Be25850	25	850	-
Be25950	25	950	-
Be15750Ze	15	750	Zetag8185
Be15750Ze.2	15	750	Zetag8185
Be15750MG	15	750	-
Be15750ZeMG	15	750	Zetag8185

2.2 Preparation of zeolite pellets

Two types of preparation techniques were used in this study. Zeolite pellets were manually extruded with a syringe and mechanically granulated with a food processor. Zeolites with the FAU framework, bentonite and the polyelectrolyte Zetag8185 were used to prepare the pellets.

2.2.1 Zeolite Y

Zeolite Y has the FAU structure. This zeolite type has a 12-ring pore opening with a diameter of 7.4 Å and a supercage with a diameter of 13 Å, see Figure 2.2. The SiO_2/Al_2O_3 ratio is 500, meaning that the zeolite is hydrophobic. The zeolite powder used in this research was purchased at Tosoh, Japan.

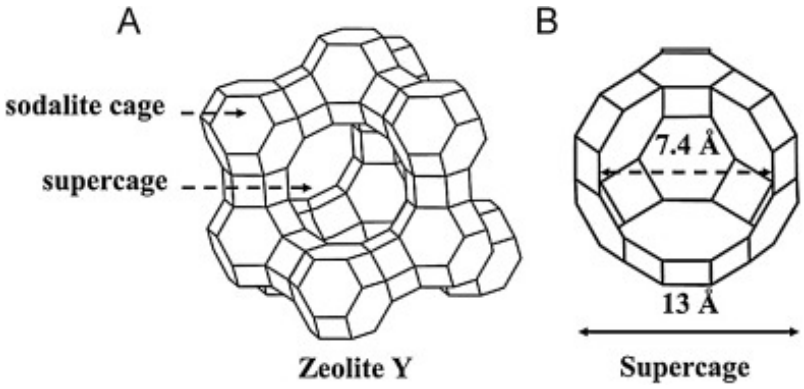

Figure 2.2: Framework structure zeolite Y

2.2.2 Extruded zeolite pellets

Zeolite FAU pellets were prepared by mixing zeolite powder, dried at 105°C, with bentonite (Sigma-Aldrich) in a weight ratio zeolite:binder = 85:15, 80:20 and 75:25. Then demineralised water or polyelectrolyte (0.2wt% in demineralised water) was added in stages. The mixture was moulded together and extruded using a syringe in strings with a diameter of 2 mm. The strings were cut in pellets with a length between 5-10 mm. The pellets were dried at 105°C for 12-24 hours. Subsequently, the pellets were calcined at 750, 850 and 950°C. The warming up time to reach the final temperature was 3 hours and the final temperature was maintained for 3 hours.

2.2.3 Granulated zeolite pellets

Zeolite FAU pellets were prepared in a food processor (Braun, MQ325). The zeolite powder was dried before use at 105°C. The zeolite powder was mixed with bentonite in a weight ratio zeolite:binder = 85:15. Then demineralised water or polyelectrolyte (0.2wt% in demineralised water) was added in stages. The mixture was mixed in the food processor until granules were formed in a size range of 1-3 mm. Subsequently, the granules were dried at 105°C for 12-24 hours and the granules were calcined at 750°C. The warming up time to reach the final temperature was 3 hours and the final temperature was maintained for 3 hours.

2.3 Wear resistance

Due to the fact that pellets were used in all different kind of fields and have different purposes, there is not a general or most used method to measure the mechanical strength of pellets. In this study the wear resistance of the zeolite pellets was measured by two tests, the jar test and the ball-pan hardness test.

The jar test was conducted in water. The pellets were placed in a beaker with baffles and stirred at a high rate. Due to the baffles, the pellets were subjected to shear stress with the moving water. The ball-pan hardness test was based on the Standard Test Method for Ball-Pan Hardness of Activated Carbon, see appendix A (ASTM D3802, 2016). The ball-pan hardness test is a dry test, where the pellets were shaken with steel balls in a closed off pan. During this test the pellets were exposed to shear stress with the steel balls. Although the tests do not reflect the shear to which the pellets are exposed to in reality, the tests are useful in establishing a measurable characteristic for the wear resistance of the pellets.

2.3.1 Jar test

The jar test (Velp JLT 6) was conducted using 2 L beakers with baffles (Figure 2.3). 2 grams of pellets and 1 L of demineralised water were used. The overhead stirrers stirred at a rate of 300 rpm for 5.5 hours. After stirring, the pellets were separated from the water and were dried at a temperature of 105°C. Subsequently, the dry pellets were sieved with a sieve size of 0.85mm and weighed.

The jar test hardness number was calculated using Equation 2.1.

$$H_j = 100\frac{B}{A} \tag{2.1}$$

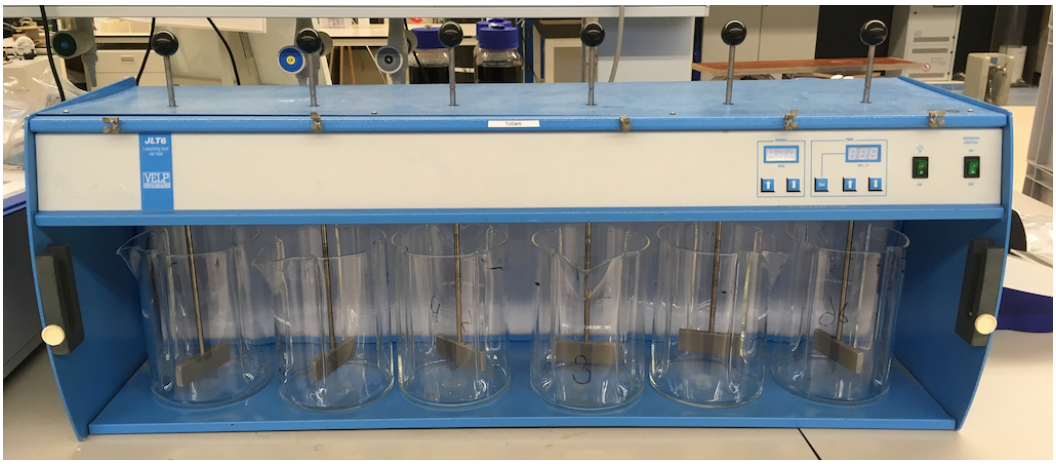

Figure 2.3: Set-up jar test

where
H_j = jar test hardness number
A = weight of initial sample $[g]$
B = weight of sample retained on sieve $[g]$

2.3.2 Ball-pan hardness test

The ball-pan hardness test was conducted with a mechanical sieve shaker (RO-TAP® RX-29) (Figure 2.4). 100 ml of pellets were weighted. The hardness test pan was placed in the mechanical sieve shaker and the weighed sample together with fifteen 12.7 mm and fifteen 9.5 mm steel balls were poured into the hardness test pan (Figure 2.5a). The sieve stack was completed by stacking five full-height sieves and the sieve cover on top of the hardness pan. The sample was shaken for 30 minutes, while being tapped by the hammer to increase extra shear stress. In Figure 2.5b the sample after shaking is shown. After the shaking period, the sieve stack was removed and a receiving pan together with the hardness test sieve was placed in the mechanical sieve shaker. The size of the hardness test sieve was 0.85mm for the extruded pellets and 0.212mm for the granulated pellets. The sample was transferred from the hardness test pan to the hardness test sieve and the five full-height sieves and sieve cover were placed on top of the hardness test sieve. The sample was shaken for 10 minutes with tapping hammer operating. The sample remaining on the hardness test sieve and the pan catch was weighed.

The hardness number was calculated using Equation 2.2.

$$H_{bp} = 100\frac{B}{A} \tag{2.2}$$

where
H_{bp} = ball-pan hardness number
A = weight of sample loaded onto hardness pan $[g]$
B = weight of sample retained on hardness test sieve $[g]$

Figure 2.4: Set-up ball-pan hardness test

(a) Hardness test pan before shaking

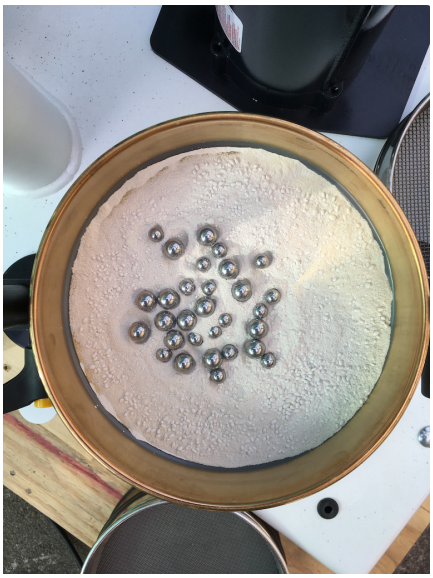

(b) Hardness test pan after shaking

Figure 2.5: Hardness test pan

2.4 Mercury intrusion porosimetry

Mercury intrusion porosimetry (MIP) is an analytical technique to determine pore size, pore volume and pore size distribution among other porosity-related aspects. Mercury, a non-wetting liquid that does not enter pores by capillary action, must be forced into a porous structure by external pressure (Figure 2.6). The pore size data is determined by the pressure that is needed for the liquid to intrude into a pore using the Washburn equation.

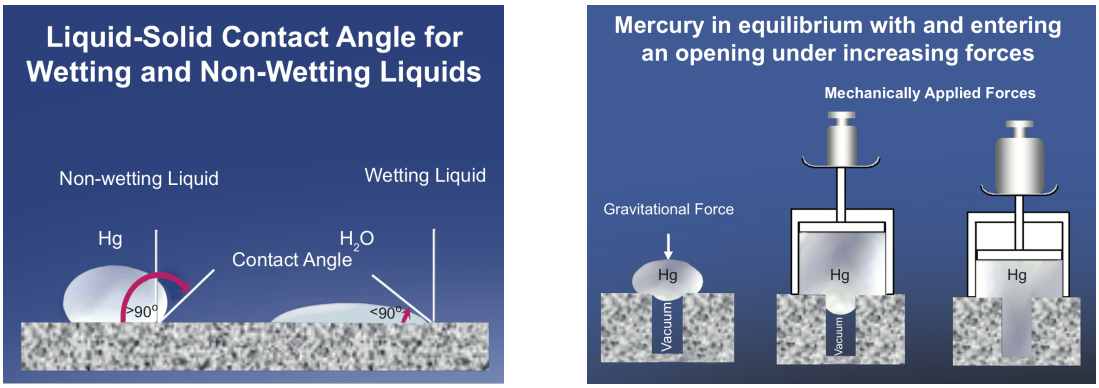

(a) Different angles of contact for wetting and non-wetting liquids

(b) Mercury does not penetrate pores by capillary, but must be forced by external pressure

Figure 2.6: Principle of mercury intrusion porosimetry (Micromeritics Instrument Corporation, 2018)

The Washburn equation:

$$-\pi D\gamma cos\theta = \frac{\pi D^2 P}{4} \tag{2.3}$$

where

D = pore diameter $[m]$
γ = surface tension of intrusion liquid $[N/m]$
θ = contact angle of intrusion liquid $[°]$
P = external pressure $[Pa]$

The relationship between applied pressure and the minimum pore size into which mercury will be forced to enter is:

$$D = -4\gamma cos\theta / P \tag{2.4}$$

The required pressure to force the mercury into the pores is inversely proportional to the size of the pores. Meaning that with increasing pressure smaller pores are intruded with mercury.

The pore size distribution of the pellets was determined with MIP instrument Micromeritics AutoPore IV 9500. In this research, the surface tension, γ, and the contact angle, θ, were set to 0.485 and 141, respectively.

2.5 Methylene blue adsorption

2.5.1 Methylene blue

Methylene blue is an odourless compound that consists of dark green crystals. Solutions of methylene blue in water have a deep blue colour. Methylene blue can be used as indicator for adsorption capacity of zeolites and is measured with spectroscopy. The properties of methylene blue are shown in Table 2.5. One of the advantages of methylene blue is the high solubility in water, enabling high initial concentrations for adsorption experiments. This allows for short-term experiments of a few days. In addition, the molecular diameter matches the pore diameter of zeolite Y.

Table 2.5: Properties of methylene blue

Compound	Chemical formula	Molar mass (g/mol)	Solubility (mg/L)	Molecular diameter Å
Methylene blue	$C_{16}H_{18}ClN_3S$	373.9	43600	5-8

2.5.2 Batch experiments

Methylene blue adsorption experiments were conducted to obtain the LDF kinetic rate constants. The experiments were conducted in 1 L cylindrical glass reactors. The initial methylene blue concentration was 250 mg/L. The amount of pellets was 588 mg/L methylene blue solution. Samples were taken three times a day for 4 days. At every time a 2 mL sample was taken using a syringe and filtered (Chromafil^{TM} Xtra PES-45/25). Subsequently, a 0.2 mL sample was taken from the 2 mL sample and added to a 12 mL test tube. The last sample was diluted 50x with demineralised water to 10 mL. The methylene blue was analysed by measuring absorbance at a wavelength of $\lambda = 665$ nm with a spectrophotometer (Genesys 6) and computing from the calibration curve (see appendix B).

2.6 Modelling breakthrough

2.6.1 The linear driving force model

The adsorption of OMPs on zeolites is assumed to be mass transfer controlled. The mass balance, which describes the mass transfer of compounds through the filter bed, is given in Equation 2.5:

$$\frac{\delta C}{\delta t} = D_L \frac{\delta^2 C}{\delta z^2} - v\frac{\delta C}{\delta z} - \frac{1-\varepsilon_b}{\varepsilon_b}\rho_{ads}\frac{\delta q}{\delta t} \tag{2.5}$$

where

C = dissolved OMP concentration $[g/L]$
t = time $[s]$
D_L = axial dispersion coefficient $[m^2/s]$
q = loading $[mg/g]$
z = longitudinal distance in the filter bed $[m]$
v = interstitial liquid velocity $[m/h]$

ε_b = fixed bed porosity $[-]$
ρ_{ads} = adsorbent density $[kg/m^3]$

The LDF model is a simplified model wherein an overall kinetic rate constant is used (Sharma et al., 2003). The LDF equation is given by:

$$\frac{\delta q}{\delta t} = k(q_e - q) \tag{2.6}$$

where
k = LDF kinetic rate constant $[1/s]$
q_e = equilibrium loading $[mg/g]$
q = loading $[mg/g]$

The breakthrough curve is plotted by solving Equation 2.5 and Equation 2.6. The two partial differential equations were solved using COMSOL Multiphysics® Modelling Software by T.K. Liu (Liu, 2017).

In COMSOL the input parameters were adjusted to fit the data used in this research and include parameters specific for the zeolite pellets, operational data and parameters specific for methylene blue adsorption by the zeolite pellets.

The particle density (ρ_p) of the zeolite pellets was determined by measuring the volume and weight of 10 pellets. For each pellet the particle density was calculated and the average of the 10 pellets was taken. The bulk density (ρ_b) was determined by filling a 250mL graduated cylinder. The fixed bed porosity (ε_b) was calculated by Equation 2.7.

$$\varepsilon_b = 1 - \frac{\rho_b}{\rho_p} \tag{2.7}$$

The operational data, consisting of the bed length (L) and interstitial velocity (v) (Equation 2.8), was adjusted to fit an empty bed contact time (EBCT) of 1, 5 and 20 minutes (Equation 2.9).

$$v = \frac{v_0}{\varepsilon_b} \tag{2.8}$$

$$EBCT = \frac{L}{v_0} \tag{2.9}$$

The axial dispersion coefficient (D_L) for a fixed bed column packed with particles can be determined experimentally (Heijman et al., 2002). However, during this study fixed bed column experiments were not conducted and therefore the axial dispersion coefficient was not determined and the coefficient used in the study of T.K. Liu was taken (Liu, 2017).

Methylene blue isotherm adsorption experiments were conducted by M. Fu (PhD student, Sanitary Engineering, TU Delft) to determine the Freundlich isotherm (see appendix B). The Freundlich constants K_F and n were determined by plotting log q_e versus log C_e.

The breakthrough curve was simulated with a methylene blue initial concentration of 1 mg/L. Although the methylene blue experiments were conducted with an initial concentration of

250 mg/L, a lower initial concentration was chosen to approach the OMP concentrations in wastewater.

The LDF kinetic rate constant was determined with Equation 2.6. Using the Freundlich isotherm (Equation 1.1), the LDF equation (Equation 2.6) was transformed in terms of concentration as (Heijman et al., 2002):

$$C = (C_0 - C_e)e^{-kt} + C_e \tag{2.10}$$

In logarithmic form:

$$ln\frac{C - C_e}{C_0 - C_e} = -kt \tag{2.11}$$

where
C = concentration$[mg/L]$
C_0 = initial concentration $[mg/L]$
C_e = equilibrium concentration $[mg/L]$
k = LDF kinetic rate constant $[1/s]$
t = time $[s]$

The LDF kinetic rate constant was determined by plotting $ln\frac{C-C_e}{C_0-C_e}$ versus the time, t. The slope of the straight line is the LDF kinetic rate constant, k.

A summary of the input parameters is shown in Table 2.6.

Table 2.6: COMSOL parameters

Parameter	Symbol	Value	Unit
Particle density	ρ_p	variable	$[kg/m^3]$
Bulk density	ρ_b	variable	$[kg/m^3]$
Fixed bed porosity	ε_b	variable	$[-]$
Bed length	L	1.5	$[m]$
Interstitial velocity	v	variable	$[m/s]$
Axial dispersion coefficient	D_L	3E-3	$[m^2/s]$
Freundlich capacity factor	K_F	41.03	$[(\frac{mg}{g})(\frac{L}{mg})^n]$
Freundlich intensity parameter	n	0.243	$[-]$
Initial concentration	C_0	1	$[mg/L]$
LDF kinetic rate constant	k	variable	$[1/s]$

Chapter 3

Results and discussion

3.1 Engineering of zeolite pellets

In the first phase, extruded pellets with three different binder percentages were prepared. These pellets were calcined at three different temperatures, resulting in nine pellets (Table 3.1). The effect of the binder content and calcination temperature on the wear resistance and pore size distribution of the pellets was analysed.

Table 3.1: Overview of pellets

Zeolite pellet	Binder content [%]	Temperature [°C]
Be15750	15	750
Be15850	15	850
Be15950	15	950
Be20750	20	750
Be20850	20	850
Be20950	20	950
Be25750	25	750
Be25850	25	850
Be25950	25	950

3.1.1 Wear resistance

The effect of the binder content and temperature on the wear resistance of the pellets was determined by the jar test and ball-pan hardness test. The results of these tests are shown in Figure 3.1 and Figure 3.2. The figures show the amount of pellets, in percentage, which were more than half the size of the smallest nominal particle size after testing. The pellet with the lowest binder content (15%) and temperature (750°C) was chosen as reference point, indicated by 0% in Table 3.2 and Table 3.3. The effect of the binder content on the wear resistance was determined by comparing the hardness number of the pellets with the three different binder contents calcined at the same temperature, for each temperature. Whereas the effect of the temperature was determined by comparing the pellets calcined at the three different temperatures with the same binder content, for each binder content.

Jar test

The jar test showed only a small difference between the pellets, varying between a hardness number of 91.3 and 93.5 (Figure 3.1). In Table 3.2 the increase or decrease, in percentage, for each pellet configuration compared to the reference point is shown.

The results showed no relation between the hardness number and increasing the temperature. Increasing the binder content resulted in an increase in hardness number for both the pellets calcined at 850°C and 950°C.

Since the results do not show considerable differences between the pellet configurations and no clear relations were identified, the jar test was not considered to be a useful strength test.

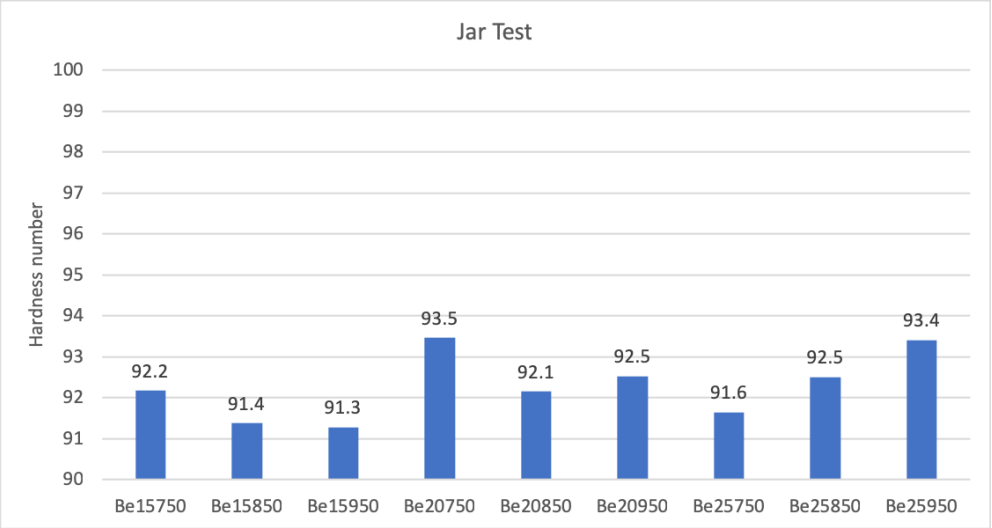

Figure 3.1: Jar hardness number: different pellet configurations to test the effect of the binder content and temperature

Table 3.2: Increase or decrease of jar hardness number compared to reference point

Binder content [%] \ Temperature [°C]	750	850	950
15	0%	-0.86%	-0.96%
20	1.41%	-0.02%	0.39%
25	-0.57%	0.36%	1.34%

Ball-pan hardness test

The ball-pan hardness test showed a clear relation between the temperature and wear resistance and between the binder percentage and wear resistance (Figure 3.2). In Table 3.3 the increase, in percentage, for each pellet configuration compared to the reference point is shown.

Table 3.3 shows that the increase of the binder content in the pellets resulted in an increase in hardness number. Only for the binder content of 25% at 750°C the hardness

number decreases compared to the pellet with 20% binder content. The effect was most noticeable between the 15% and 20%. For 750°C the hardness number was almost 2 times higher for 20% than for 15%. The increase in hardness number between the binder content of 20% and 25% was compared to the change of hardness number between 15% and 20% very small.

The increase of the temperature resulted in an increase in hardness number for all binder contents. The effect was larger from 750°C to 850°C than from 850°C to 950°C.

The ball-pan hardness number of the zeolite pellets varied between 28.7 and 82.5. In comparison, the ball-pan hardness number of activated carbon, used at several Dutch and Belgian drinking water companies, varies between 60.9 and 94.3 (Vries et al., 2012). This indicates that zeolite pellets with sufficient wear resistance could be engineered.

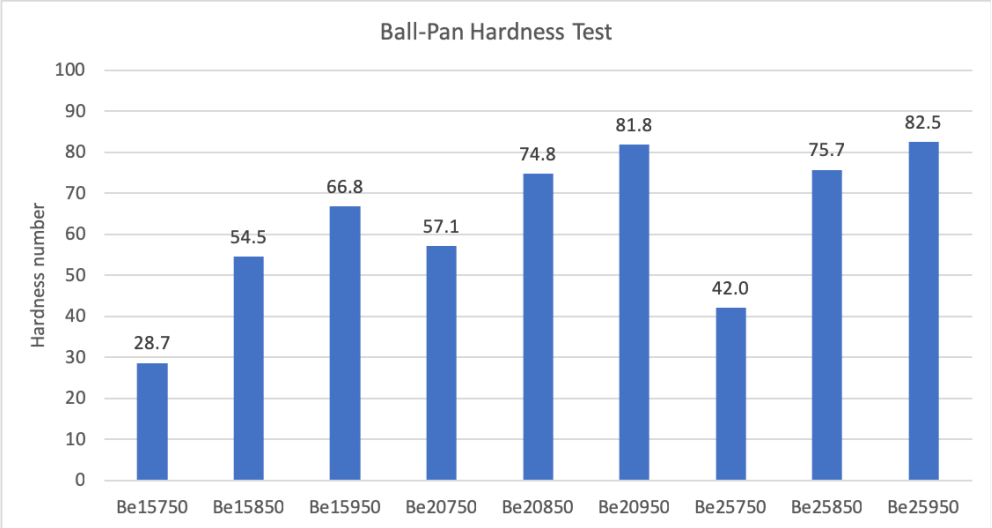

Figure 3.2: Ball-pan hardness number: different pellet configurations to test the effect of the binder content and temperature

Table 3.3: Increase or decrease of ball-pan hardness number compared to reference point

Binder content [%] \ Temperature [°C]	750	850	950
15	0%	90%	133%
20	99%	161%	185%
25	47%	164%	188%

3.1.2 Porosity

The effect of the binder content and temperature on the porosity of the pellets is shown in Figure 3.3. The pore size distributions of the pellets showed a high peak around $0.02\mu m$ and a smaller peak at $0.14\mu m$. The percentage of the pore volume with a minimum pore size of $0.05\mu m$ (macropores), $0.5\mu m$ and $1\mu m$ is given in Table 3.4.

The table shows that around 80% of the pore volume in the pellets was generated by pores with a minimum pore size of $0.05\mu m$. This means that the majority of the total pore volume

consisted of macropores. The main difference between the pellets was the percentage pore volume with pores larger than $0.5\mu m$. The pellets with a higher temperature had a larger percentage pore volume with a minimum pore size of $0.5\mu m$. The increase in binder content also showed a small increase in pore volume. The effect was less for the minimum pore size of $1\mu m$, although still present.

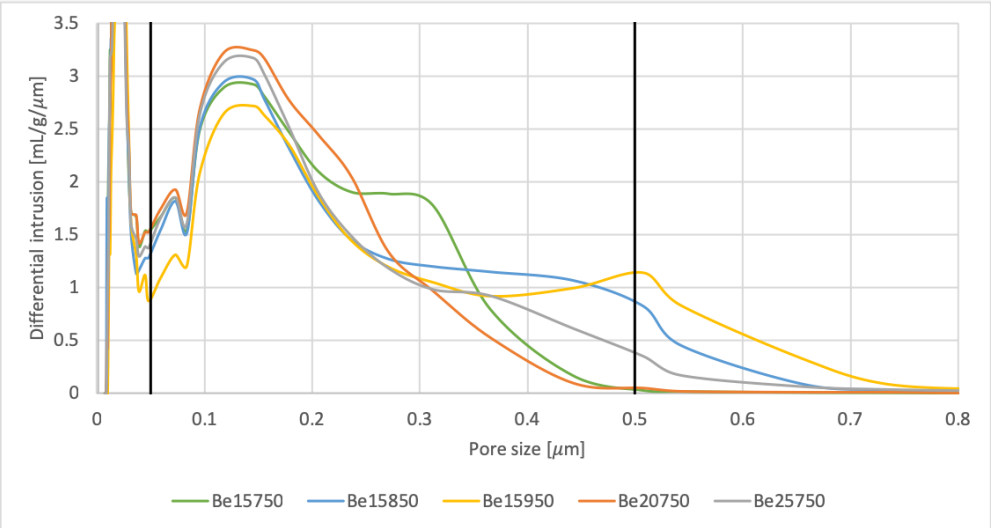

Figure 3.3: Pore size distribution of the different pellet configurations

Table 3.4: The percentage pore volume with a minimum pore size of 0.05, 0.5 and $1\mu m$, respectively

	$> 0.05\mu m$	$> 0.5\mu m$	$> 1\mu m$
Be15750	79.9%	1.4%	0.3%
Be15850	81.1%	13.2%	0.7%
Be15950	82.3%	20.9%	1.0%
Be20750	79.3%	1.4%	0.3%
Be25750	80.2%	7.8%	0.9%

3.1.3 Conclusion

Based on the results, one pellet configuration was chosen to be used in the next stages of this research. The jar test did not show a relation between the temperature and wear resistance and the influence of the binder content on the wear resistance was only minimal. The mercury intrusion porosimetry results did show a relation between the temperature and porosity and in lesser extent between the binder content and porosity for a minimum pore size of $> 0.5\mu m$. However, the effect was less for pores larger than $> 1\mu m$. Since the results did not give consistent results, it was decided to use the pellet with the lowest binder content, 15%, and the lowest temperature, 750°C. It must be noted that the results from the ball-pan hardness test were not included in this decision, since the ball-pan hardness test was not conducted at that specific moment.

3.2 Introduction of polymer to zeolite pellets

The chosen pellet, Be15750, was both prepared by extrusion as by granulation and in both pellets the polymer Zetag8185 was introduced. The 4 different pellet configurations are shown in Table 3.5. The relation between wear resistance and porosity was analysed and the LDF kinetic rate constant was determined.

Table 3.5: Overview of pellets

Zeolite pellet	Binder content [%]	Temperature [°C]	Polymer
Be15750	15	750	-
Be15750Ze	15	750	Zetag8185
Be15750 MG	15	750	-
Be15750Ze MG	15	750	Zetag8185

3.2.1 Wear resistance versus porosity

The results of the ball-pan hardness test, shown in Figure 3.4, showed that the introduction of the polymer had a contradicting effect on the wear resistance for the two preparation techniques.

The extruded pellets without polymer had a hardness number of 28.7 and with polymer of 3.5. The introduction of the polymer resulted in an increase in porosity, as can be seen in Figure 3.5, which explains the decrease of the wear resistance of the pellet.

The opposite effect was observed for the granulated pellets. The pellets without polymer had a hardness number of 12.7 and with polymer 46.4. The pore size distribution showed, again, that the pellets with a lower hardness number had a larger porosity.

The fact that the polymer had opposite effects could be explained by the method of preparation. For the extruded pellets, the polymer solution was added to the zeolite-binder mixture and mixed manually. The granulated pellets were prepared in a food processor with higher shear stresses. When the unfolded polymer was subjected to strong mixing, the chains of the polymer could be damaged (Korving, 2013). It could also be possible that during the preparation of the polymer solution the chains had not completely unfolded or were already damaged.

Table 3.6: The percentage pore volume with a minimum pore size of 0.05, 0.5 and 1μm, respectively

	$> 0.05\mu m$	$> 0.5\mu m$	$> 1\mu m$
Be15750	79.9%	1.4%	0.3%
Be15750Ze	82.3%	30.9%	4.5%
Be15750 MG	67.4%	3.0%	1.6%
Be15750Ze MG	67.8%	0.9%	0.5%

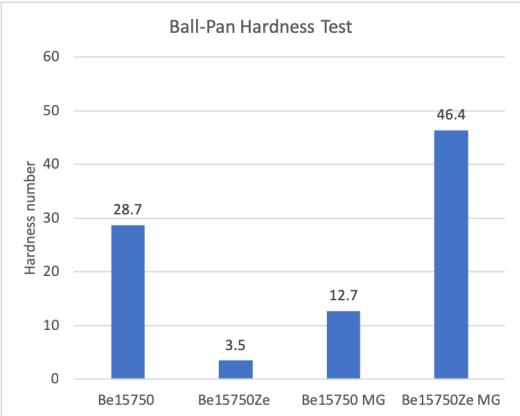

Figure 3.4: Ball-pan hardness number: Extruded and granulated pellets with and without polymer

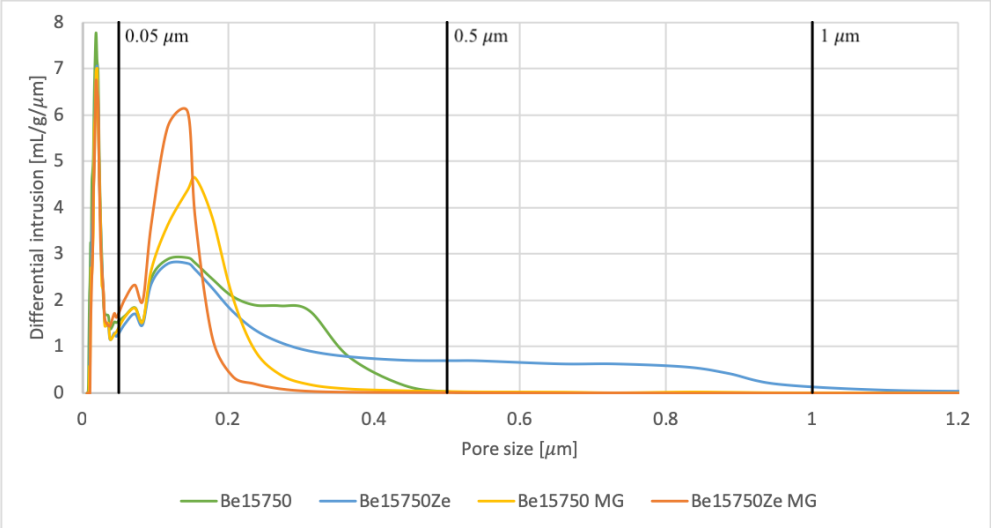

Figure 3.5: Pore size distribution of extruded and granulated pellet with and without polymer

3.2.2 The linear driving force kinetic rate constant

The effect of the two preparation techniques and the introduction of polymer on the adsorption kinetics is presented in Figure 3.6 and Figure 3.7. The figures show that the granulated pellets without polymer were the most efficient in adsorbing methylene blue, followed by the extruded pellets with polymer, granulated pellets with polymer and the extruded pellets without polymer, respectively. The LDF kinetic rate constant, k, and correlation coefficient, R^2, are shown in Table 3.7.

From the figures, one would expect that the extruded pellets with polymer (Be15750Ze) have the highest kinetic rate constant. As said before, this is not the case and could be explained by two reasons.

First of all, the methylene blue adsorption experiments were conducted by two people and due to a misunderstanding, the experiments with the extruded and granulated pellets

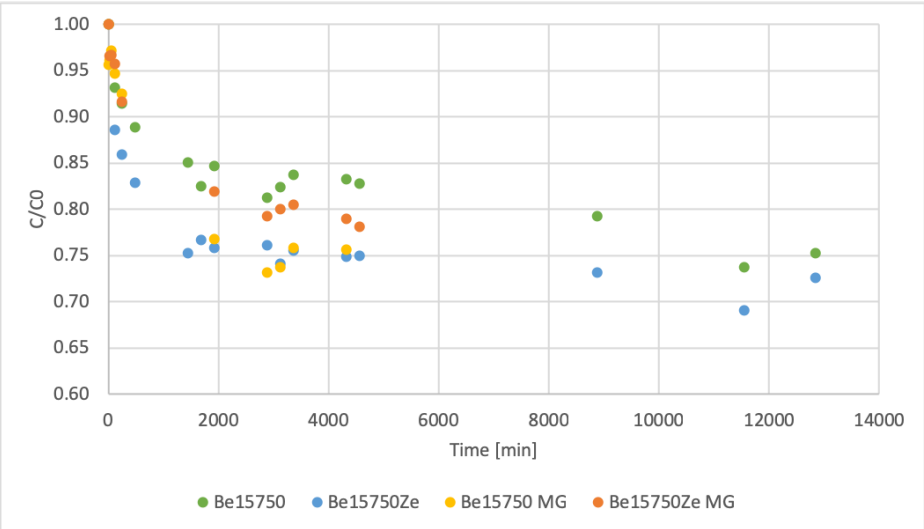

Figure 3.6: Adsorption of methylene blue to the extruded and granulated pellets with and without polymer

were not conducted in the same way. As can be seen in the figures, the samples of the granulated pellets were taken for a shorter amount of time. Therefore, it remains unknown if the granulated pellets would also show the same flattening as the extruded pellets later in time.

Second, the correlation coefficient of the extruded pellet with polymer of 0.08 cannot go unnoticed. If only the same sample points as the granulated pellets would have been used, the correlation coefficient would have shown a better fit and the kinetic rate constant would have been higher.

It would be of interest to repeat the experiments to investigate whether a later sample time would alter the results and the correlation coefficient would show a better fit.

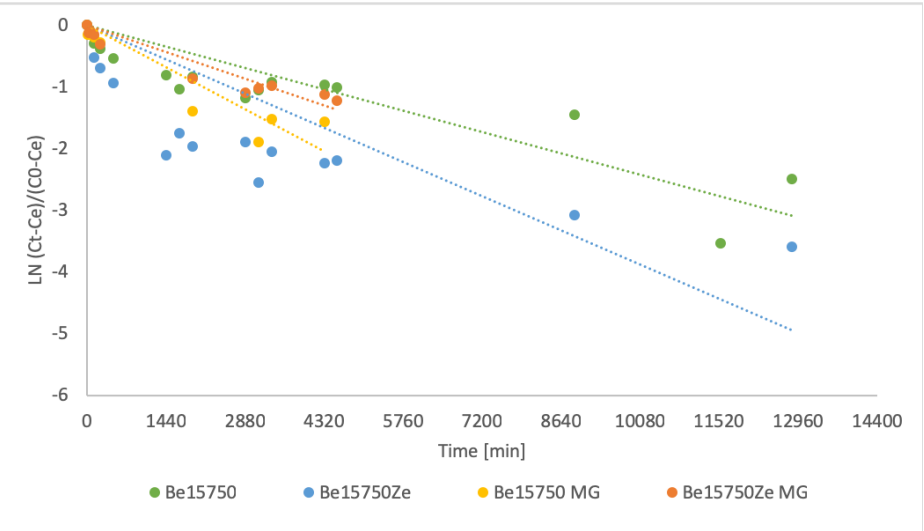

Figure 3.7: The slope of the linear trend lines determine the LDF kinetic rate constant

Table 3.7: LDF kinetic rate constants of MB and correlation coefficients for extruded and granulated pellets with and without polymer

	LDF kinetic rate constant, k $[1/s]$	Correlation coefficient, R^2
Be15750	4.00E-6	0.74
Be15750Ze	6.42E-6	0.08
Be15750 MG	7.88E-6	0.86
Be15750Ze MG	5.02E-6	0.89

The study of T.K. Liu showed that the kinetic rate constants of several OMPs adsorbed to granular activated carbon were in the same range as the kinetic rate constants found in this study (Liu, 2017). However, another study showed kinetic rate constants in the range of 6.0E-4 - 1.2E-3 for methylene blue adsorption to zeolites (Rida et al., 2013). These faster adsorption kinetics could be explained by the fact that zeolite powder instead of pellets was used for the adsorption of methylene blue (Yener et al., 2008). It could also be that the zeolite type used in the mentioned study has more affinity for the adsorption of methylene blue than the zeolite type used in this study.

3.2.3 Duplicates

The extruded pellets were made in duplicate to check for reproducibility. The duplicated pellets were subjected to the same experiments: the ball-pan hardness test, the porosity test and the methylene blue adsorption test. Only the ball-pan hardness test was not conducted for the duplicated pellet with polymer (Be15750Ze.2). The results of all the experiments are shown in appendix C.

3.3 Modelling of breakthrough

The LDF kinetic rate constants from the previous section were used to simulate the breakthrough curve and the influence of the properties of the pellets was analysed.

3.3.1 Breakthrough curves

In Figure 3.8, Figure 3.9 and Figure 3.10 the breakthrough curves with an EBCT of 20, 5 and 1 minutes are shown. The breakthrough was simulated for an initial methylene blue concentration of 1 mg/L. The properties of the zeolite pellets are shown in Table 3.8. It must be noted that the LDF kinetic rate constants of Be15750 and Be15750Ze were the average rate constants calculated from the duplicates.

For high EBCTs (20 and 5 minutes) it was found that the bulk density is related to the moment of breakthrough. A higher bulk density of the pellets in a column caused a later breakthrough point. Only at an EBCT of 1 minute, the extruded pellet with polymer (low bulk density) showed a later breakthrough point than the extruded pellet without polymer (high bulk density). This could be explained by the higher kinetic rate constant of the extruded pellet with polymer.

Table 3.8: Properties of the zeolite pellets and the variable input parameters used in COMSOL to simulate breakthrough

	LDF kinetic rate constant $[1/s]$	Bulk density $[kg/m^3]$	Particle density $[kg/m^3]$
Be15750	3.43E-6	329	582
Be15750Ze	7.26E-6	266	470
Be15750 MG	7.88E-6	347	706
Be15750Ze MG	5.02E-6	402	585

The figures show that the breakthrough of the granulated pellets occurred at a later time than the extruded pellets for all EBCTs (20, 5 and 1 minute). This could be explained by the fact that the granulated pellets have a lower porosity (Figure 3.5) and granulated pellets are spherically-shaped and therefore fit closer together than the rod-shaped pellets (extruded pellets) resulting in a higher bulk density (Kyrylyuk and Philipse, 2011).

Another interesting finding was that when the EBCT is changed to 5 and 1 minute, the LDF kinetic rate constant got of more importance. The pellets with higher kinetic rate constants shifted closer to the pellets with lower kinetic rate constants. This characteristic is further clarified in appendix D, where the three variables were analysed independently of each other.

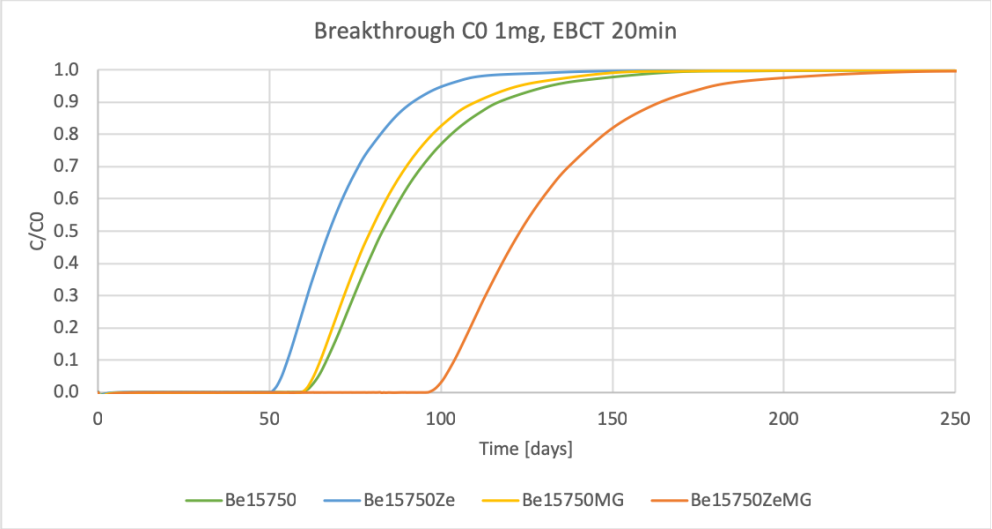

Figure 3.8: Breakthrough curves at EBCT of 20 minutes

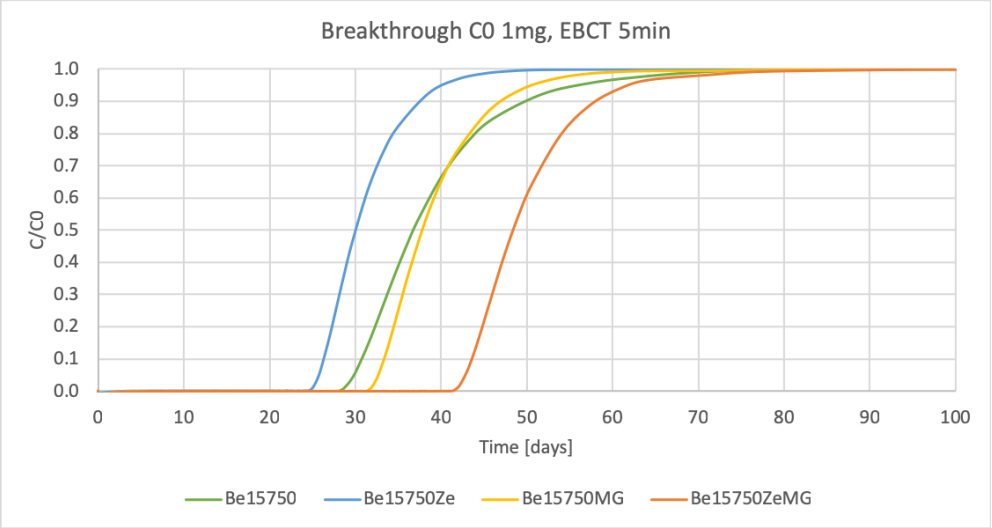

Figure 3.9: Breakthrough curves at EBCT of 5 minutes

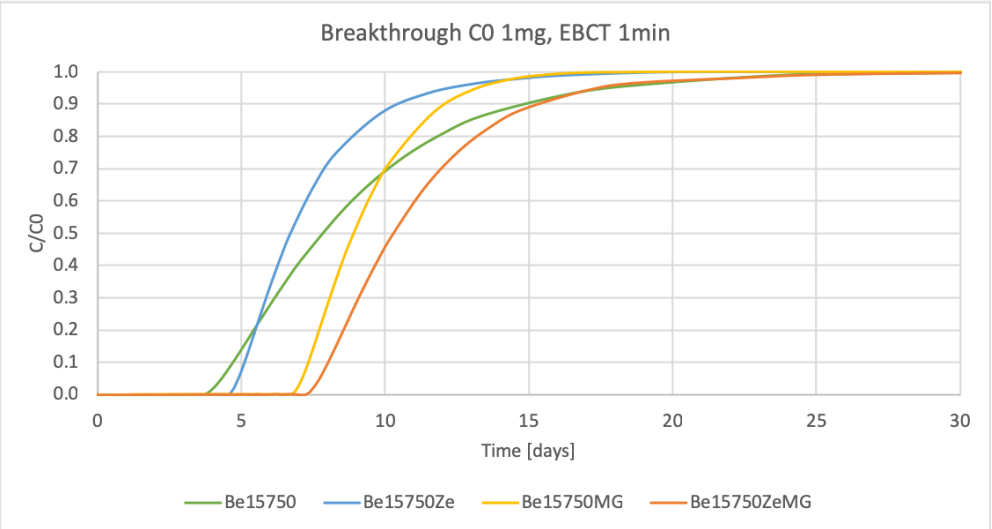

Figure 3.10: Breakthrough curves at EBCT of 1 minute

3.3.2 Limitations

Since no column breakthrough experiments have been conducted during this study, the simulated breakthrough results could not be compared and validated. In addition, various assumptions were made and will most likely have an effect on the results.

First, the initial methylene blue concentration was set at 1 mg/L, although the kinetic rate constant was determined for an initial concentration of 250 mg/L. Also, the concentration of OMPs in waste water is in the range of $ng/L - \mu g/L$. At a lower initial concentration, the breakthrough point will occur at a later time.

Second, the Freundlich constants were taken from batch experiments conducted with zeolite powder. The adsorption process depends on the particle size and therefore the particle size affects the Freundlich constants (Yener et al., 2008).

Third, the methylene blue adsorption experiments did not reach equilibrium. Therefore, the equilibrium concentration from the batch experiments with zeolite powder conducted by M. Fu (PhD student, Sanitary Engineering, TU Delft) were used. The LDF kinetic rate constant was affected by the equilibrium concentration (see equation 2.11).

Fourth, the axial dispersion coefficient was taken from a study with activated carbon as adsorbent. It is unknown whether this is a representable value for a zeolite bed.

Chapter 4

Conclusions

In this thesis several zeolite pellets were engineered to identify what properties of the zeolite pellets were important for OMP adsorption. The conclusions drawn from this study are listed below:

- Both the binder content as the calcination temperature had great influence on the wear resistance of the pellets. For both, the wear resistance increased with increasing binder content and calcination temperature.
- Both the binder content as the calcination temperature had little influence on the porosity in the zeolite pellets. The porosity increased with increasing binder content and calcination temperature, however, the effect was minimal.
- The introduction of the polyelectrolyte had opposite effect on extruded and granulated pellets. For extruded pellets, the introduction of the polyelectrolyte increased the porosity. However, the granulated pellets showed a decrease in porosity. For both preparation techniques, there was a clear relation between the porosity and the wear resistance and between the porosity and adsorption kinetics. A larger porosity decreased the wear resistance of the pellets and increased the kinetic rate constant.
- The porosity was of great importance in relation to the breakthrough. First, the porosity in the zeolite pellets determined to a great extent the bulk density of the filter bed. A higher bulk density resulted in a later breakthrough point. The bulk density was also influenced by the shape of the pellet. Spherically-shaped pellets had a higher bulk density than rod-shaped pellets. Second, as concluded above, the porosity was related to the kinetic rate constant. At lower EBCTs (5 and 1 minute), the kinetic rate constant had an influence on the breakthrough point. For these EBCTs, a higher kinetic rate constant led to a later breakthrough point.

Further research is recommended in the following fields:

- Optimization of the zeolite pellets: in this research several aspects related to the engineering process of the zeolite pellets were analysed. It was found that for extruded pellets the wear resistance was influenced by the binder content and calcination temperature. Furthermore, this study showed that the porosity and shape of the pellets had a great effect on the breakthrough. It would be of interest to find out if granulated pellets show

the same increase in wear resistance as extruded pellets and if the shape of the extruded pellets could be optimized by making them more spherically-shaped. In conclusion, an optimal balance between a high density zeolite filter bed and a high pellet porosity to increase the adsorption kinetics, but also mechanically stable zeolite pellets that can be used at an industrial scale should be found.

- Fixed bed column adsorption experiments: in this study, the breakthrough of fixed bed columns have been simulated with the LDF-model. However, the actual fixed bed column adsorption experiments have not been conducted. As a consequence, it remains unknown whether the model represents the actual situation. Therefore, it is recommended to start the column experiments and validate the LDF-model.

Bibliography

Abu-Lail, L., Bergendahl, J. A., and Thompson, R. W. (2010). Adsorption of methyl tertiary butyl ether on granular zeolites: Batch and column studies. *Journal of Hazardous Materials*, 178:363–369.

Adeel, M., Song, X., Wang, Y., Francis, D., and Yang, Y. (2017). Environmental impact of estrogens on human, animal and plant life: A critical review. *Environment International*, 99:107–119.

Arena, N., Lee, J., and Clift, R. (2016). Life Cycle Assessment of activated carbon production from coconut shells. *Journal of Cleaner Production*, 125:68–77.

ASTM D3802 (2016). Standard Test Method for Ball-Pan Hardness of Activated Carbon.

Baerlocher, C., McCusker, L. B., and Olson, D. H. (2007). *Atlas of Zeolite Framework Types*. Elsevier B.V., 6th edition.

Bolong, N., Ismail, A. F., Salim, M. R., and Matsuura, T. (2009). A review of the effects of emerging contaminants in wastewater and options for their removal. *Desalination*, 238(1-3):229–246.

Crane, M., Watts, C., and Boucard, T. (2006). Chronic aquatic environmental risks from exposure to human pharmaceuticals. *Science of the Total Environment*, 367(1):23–41.

de Jesus Gaffney, V., Almeida, C. M. M., Rodrigues, A., Ferreira, E., Benoliel, M. J., and Cardoso, V. V. (2015). Occurrence of pharmaceuticals in a water supply system and related human health risk assessment. *Water Research*, 72:199–208.

Grontmij (2011). Zuivering geneesmiddelen uit afvalwater. Technical report, Grontmij Nederland B.V., Houten.

Heijman, S. G. J., Siegers, W., Sterk, R., and Hopman, R. (2002). Prediction of breakthrough of pesticides in GAC-filters and breakthrough of colour in ion-exchange-filters. *Water Science and Technology: Water Supply*, 2(1):103–108.

Hu, J., Shang, R., Heijman, S. G. J., and Rietveld, L. C. (2015). Reuse of spent granular activated carbon for organic micro-pollutant removal from treated wastewater. *Journal of Environmental Management*, 160:98–104.

Hung, H. W. and Lin, T. F. (2006). Adsorption of MTBE from contaminated water by carbonaceous resins and mordenite zeolite. *Journal of Hazardous Materials*, 135(1-3):210–217.

Hutter, H. P., Wallner, P., Moshammer, H., Hartl, W., Sattelberger, R., Lorbeer, G., and Kundi, M. (2005). Blood concentrations of polycyclic musks in healthy young adults. *Chemosphere*, 59(4):487–492.

Jasra, R. V., Tyagi, B., Badheka, Y. M., Choudary, V. N., and Bhat, T. S. G. (2003). Effect of Clay Binder on Sorption and Catalytic Properties of Zeolite Pellets. *Industrial & Engineering Chemistry Research*, 42(14):3263–3272.

Jiang, N., Shang, R., Heijman, S. G. J., and Rietveld, L. C. (2018). High-silica zeolites for adsorption of organic micro-pollutants in water treatment: a review. *Water Research*, 144:145–161.

Kannan, K., Reiner, J. L., Se, H. Y., Perrotta, E. E., Tao, L., Johnson-Restrepo, B., and Rodan, B. D. (2005). Polycyclic musk compounds in higher trophic level aquatic organisms and humans from the United States. *Chemosphere*, 61(5):693–700.

Keleb, E. I., Vermeire, A., Vervaet, C., and Remon, J. P. (2004). Extrusion granulation and high shear granulation of different grades of lactose and highly dosed drugs: a comparative study. *Drug Development and Industrial Pharmacy*, 30(6):679–691.

Kidd, K. A., Blanchfield, P. J., Mills, K. H., Palace, V. P., Evans, R. E., Lazorchak, J. M., and Flick, R. W. (2007). Collapse of a fish population after exposure to a synthetic estrogen. *PNAS*, 104(21):8897–8901.

Korving, L. (2013). Viscositeit, geleidbaarheid en ladingsdichtheid als maat voor de rijping van polymeer. Technical report, Aiforo. Report no. AP12008-AR-01.

Kyrylyuk, A. V. and Philipse, A. P. (2011). Effect of particle shape on the random packing density of amorphous solids. *Physica Status Solidi (A) Applications and Materials Science*, 208(10):2299–2302.

Liu, T. K. (2017). *Organic Micropollutant Treatment by Pre-Ozonation and Activated Carbon*. Master thesis, Delft University of Technology.

Liu, Z., Kanjo, Y., and Mizutani, S. (2009). Removal mechanisms for endocrine disrupting compounds (EDCs) in wastewater treatment - physical means, biodegradation, and chemical advanced oxidation: A review. *Science of the Total Environment*, 407(2):731–748.

Micromeritics Instrument Corporation (2018). Mercury Intrusion Porosimetry Theory.

Mousel, D., Palmowski, L., and Pinnekamp, J. (2017). Energy demand for elimination of organic micropollutants in municipal wastewater treatment plants. *Science of the Total Environment*, 575:1139–1149.

Mueller, U., Senk, R., Harder, W., Rudolf, P., and Rieber, N. (2006). EP Patent 1368118B1.

Petrovi, M., Gonzalez, S., and Barceló, D. (2003). Analysis and removal of emerging contaminants in wastewater and drinking water. *Trends Anal. Chem.*, 22(10):685–696.

Rida, K., Bouraoui, S., and Hadnine, S. (2013). Adsorption of methylene blue from aqueous solution by kaolin and zeolite. *Applied Clay Science*, 83-84:99–105.

Rivera-Utrilla, J., Sánchez-Polo, M., Ferro-García, M. Á., and Prados-Joya, G. (2013). Pharmaceuticals as emerging contaminants and their removal from water. A review. *Chemosphere*, 93(7):1268–1287.

Rossner, A., Snyder, S. A., and Knappe, D. R. U. (2009). Removal of emerging contaminants of concern by alternative adsorbents. *Water Research*, 43(15):3787–3796.

Ruthven, D. M. (1984). Microporous Adsorbents. In *Principles of adsorption and adsorption processes*. John Wiley & Sons.

Schumann, K., Unger, B., Brandt, A., and Scheffler, F. (2012). Investigation on the pore structure of binderless zeolite 13x shapes. *Microporous and Mesoporous Materials*, 154:119–123.

Schwab, B. W., Hayes, E. P., Fiori, J. M., Mastrocco, F. J., Roden, N. M., Cragin, D., Meyerhoff, R. D., D'Aco, V. J., and Anderson, P. D. (2005). Human pharmaceuticals in US surface waters: A human health risk assessment. *Regulatory Toxicology and Pharmacology*, 42(3):296–312.

Schwarzenbach, R. P., Escher, B. I., Fenner, K., Hofstetter, T. B., Johnson, C. A., von Gunten, U., and Wehrli, B. (2006). The Challenge of Micropollutants in Aquatic Systems. *Science*, 313:1072–1077.

Sextl, E., Roland, E., Kleinschmidt, P., and Kiss, A. (1994). US Patent 5316993.

Sharma, S. K., Petrusevski, B., Heijman, B. G. J., and Schippers, J. C. (2003). Prediction of iron (II) breakthrough in adsorptive filters under anoxic conditions. *Journal of Water Supply: Research and Technology-Aqua*, 52(8):529–544.

Stackelberg, P. E., Gibs, J., Furlong, E. T., Meyer, M. T., Zaugg, S. D., and Lippincott, R. L. (2007). Efficiency of conventional drinking-water-treatment processes in removal of pharmaceuticals and other organic compounds. *Science of the Total Environment*, 377(2-3):255–272.

STOWA (2014). Microverontreinigingen in het water — Een Overzicht. Technical report, Stichting Toegepast Onderzoek Waterbeheer. Report no. 2014-45, Amersfoort.

Tchobanoglous, G., Burton, F. L., and Stensel, H. D. (2003). *Wastewater engineering, treatment and reuse*. McGraw-Hill, 4th edition.

Tetreault, G. R., Bennett, C. J., Shires, K., Knight, B., Servos, M. R., and McMaster, M. E. (2011). Intersex and reproductive impairment of wild fish exposed to multiple municipal wastewater discharges. *Aquatic Toxicology*, 104(3-4):278–290.

Tijani, J. O., Fatoba, O. O., and Petrik, L. F. (2013). A review of pharmaceuticals and endocrine-disrupting compounds: Sources, effects, removal, and detections. *Water, Air, and Soil Pollution*, 224(11).

Vethaak, A. D., Rijs, G. B. J., Schrap, S. M., Ruiter, H., Gerritsen, A., and Lahr, J. (2002). Estrogens and xeno-estrogens in the aquatic environment of the Netherlands. Occurrence, Potency and Biological Effects. Technical report, Institute for Inland Water Management

and Waste Water Treatment (RIZA) and Institute for Coastal and Marine Management (RIKZ). RIZA/RIKZ-report no. 2002.001.

Vries, D., Hofman-Caris, R., and Post, J. (2012). Stuurparameters Actieve Kool, Deelrapport 2: Overzicht koolkarakteristieken bij Nederlandse en Vlaamse drinkwaterbedrijven. Technical Report April.

Yener, J., Kopac, T., Dogu, G., and Dogu, T. (2008). Dynamic analysis of sorption of Methylene Blue dye on granular and powdered activated carbon. *Chemical Engineering Journal*, 144(3):400–406.

Yonli, A. H., Batonneau-Gener, I., and Koulidiati, J. (2012). Adsorptive removal of α-endosulfan from water by hydrophobic zeolites. An isothermal study. *Journal of Hazardous Materials*, 203-204:357–362.

Yunlong, L., Wenshan, G., Huu Hao, N., Long Duc, N., Faisal Ibney, H., Jian, Z., and Shuang, L. (2014). A review on the occurrence of micropollutants in the aquatic environment and their fate and removal during wastewater treatment. *Science of the Total Environment*, 473-474(March):619–641.

Zhang, Y., Mancke, R. G., Sabelfeld, M., and Geißen, S. U. (2014). Adsorption of trichlorophenol on zeolite and adsorbent regeneration with ozone. *Journal of Hazardous Materials*, 271:178–184.

Zietzschmann, F., Stützer, C., and Jekel, M. (2016). Granular activated carbon adsorption of organic micro-pollutants in drinking water and treated wastewater - Aligning breakthrough curves and capacities. *Water Research*, 92:180–187.

Appendix A

Standard Test Method for Ball-Pan Hardness of Activated Carbon

Designation: D3802 – 16

Standard Test Method for Ball-Pan Hardness of Activated Carbon[1]

This standard is issued under the fixed designation D3802; the number immediately following the designation indicates the year of original adoption or, in the case of revision, the year of last revision. A number in parentheses indicates the year of last reapproval. A superscript epsilon (ε) indicates an editorial change since the last revision or reapproval.

1. Scope

1.1 This test method covers a procedure for determining the ball-pan hardness number of granular activated carbons. For the purpose of this test, granular activated carbons are those having particles 90 % of which are larger than 80 mesh (180 μm) as determined by Test Method D2862.

1.2 The values stated in SI units are to be regarded as standard. No other units of measurement are included in this standard.

1.3 *This standard does not purport to address all of the safety concerns, if any, associated with its use. It is the responsibility of the user of this standard to establish appropriate safety and health practices and determine the applicability of regulatory limitations prior to use.*

2. Referenced Documents

2.1 *ASTM Standards:*[2]

B19 Specification for Cartridge Brass Sheet, Strip, Plate, Bar, and Disks

B150/B150M Specification for Aluminum Bronze Rod, Bar, and Shapes

D2652 Terminology Relating to Activated Carbon

D2854 Test Method for Apparent Density of Activated Carbon

D2862 Test Method for Particle Size Distribution of Granular Activated Carbon

D2867 Test Methods for Moisture in Activated Carbon

E11 Specification for Woven Wire Test Sieve Cloth and Test Sieves

E300 Practice for Sampling Industrial Chemicals

3. Terminology

3.1 *General*—Terms applicable to this standard are defined in Terminology D2652.

3.2 *Definitions of Terms Specific to This Standard:*

3.2.1 *nominal particle size: natural, granular, and irregularly shaped particle carbons*—that particle size range, expressed in terms of Specification E11 sieve sizes, whose small end excludes not more than 5 % of the particle size distribution, and whose large end excludes not more than 5 % of the distribution, on a weight basis.

3.2.2 *nominal particle size: pelleted carbons*—that particle size range, expressed in terms of Specification E11 sieve sizes, whose small end excludes not more than 10 % of the particle size distribution, and whose large end excludes not more than 5 % of the distribution, on a weight basis.

3.2.3 *small end nominal particle size*—that particle size, expressed by its equivalent Specification E11 sieve, which defines the excluded portion of the particle size distribution at its small particle size end in accordance with 3.2.1 or 3.2.2.

4. Summary of Test Method

4.1 A screened and weighed sample of the carbon is placed in a special hardness pan with a number of stainless steel balls, then subjected to a combined rotating and tapping action for 30 min. At the end of this period, the amount of particle size degradation is determined by measuring the quantity of carbon, by weight, which is retained on a sieve whose openings are closest to one half the openings of the sieve that defines the minimum nominal particle size of the original sample.

5. Significance and Use

5.1 Several methods have been employed in the past for determining the resistance of activated carbons to particle size degradation under service conditions, including the ball-pan method, the stirring bar method, and the dust elutriation method. None of these has proved completely satisfactory for all applications, and all have been questioned by ASTM Committee D28 on Activated Carbon as tests for establishing degradation resistance. However, the ball-pan method has been used widely in the past and has a broad history in the activated carbon industry for measuring the property loosely described as "hardness." In this context the test is useful in establishing a measurable characteristic of a carbon. Conceding the fact that the test does not actually measure in-service resistance to degradation, it can be used to establish the comparability of lots ostensibly of the same grade of carbon.

[1] This test method is under the jurisdiction of ASTM Committee D28 on Activated Carbon and is the direct responsibility of Subcommittee D28.04 on Gas Phase Evaluation Tests.

Current edition approved June 1, 2016. Published July 2016. Originally approved in 1979. Last previous edition approved in 2010 as D3802 – 10. DOI: 10.1520/D3802-16.

[2] For referenced ASTM standards, visit the ASTM website, www.astm.org, or contact ASTM Customer Service at service@astm.org. For *Annual Book of ASTM Standards* volume information, refer to the standard's Document Summary page on the ASTM website.

APPENDIX A. STANDARD TEST METHOD FOR BALL-PAN HARDNESS OF ACTIVATED CARBON

TABLE 1 Hardness Test Sieve (HTS) Corresponding to Specification E11 Sieves Defining Small-End Nominal Particle Size (SNPS)

SNPS		HTS		SNPS		HTS	
Opening, mm	E11 Mesh	Opening, µm	E11 Mesh	Opening, µm	E11 Mesh	Opening, µm	E11 Mesh
5.6	3½	2800	7	850	20	425	40
4.75	4	2360	8	710	25	355	45
4.00	5	2000	10	600	30	300	50
3.35	6	1700	12	500	35	250	60
2.80	7	1400	14	425	40	212	70
2.36	8	1180	16	355	45	180	80
2.00	10	1000	18	300	50	150	100
1.70	12	850	20	250	60	125	120
1.40	14	710	25	212	70	106	140
1.18	16	600	30	180	80	90	170
1.00	18	500	35				

6. Apparatus and Materials

6.1 *Mechanical Sieve Shaker,* designed to produce from 140 to 160 taps and from 280 to 320 rotating motions per minute in a stack of standard Specification E11 sieves.[3] Adjust the sieve shaker to accommodate the desired number of sieves, receiver pan, and sieve cover. Adjust the bottom stops to give a clearance of approximately 1.6 mm between the bottom plate and the sieves so that the sieves will be free to rotate. Fit the cover plate with a cork stopper which extends from 3.2 to 9.5 mm above the metal recess.

6.2 *Wire Cloth Sieves,* in accordance with Specification E11; six required, at least four of which bracket the expected nominal particle size distribution of the sample, and one of which, designated the hardness test sieve, has an opening as close as possible to one half the opening of the sieve that defines the smaller nominal particle size of the original sample. Table 1 lists the hardness test sieve corresponding to each minimum nominal sieve.

6.3 *Bottom Receiver Pan and Top Sieve Cover* (see 6.1).

6.4 *Hardness Test Pan,* having the dimensions of that in Fig. 1.

6.5 *Adjustable Interval Timer,* with a precision of at least ±5 s, duration at least 600 s (10 min).

6.6 *Sample Splitter,* single-stage riffle type, in accordance with 30.5.2 of Practice E300.

6.7 *Balance,* with sensitivity and accuracy of at least 0.1 g.

6.8 *Soft Brass-Wire Brush.* [4]

6.9 *Steel Balls,* fifteen 12.7 ± 0.1 mm in diameter and fifteen 9.5 ± 0.1 mm in diameter.

7. Sampling

7.1 Guidance in sampling granular activated carbon is given in Practice E300.

[3] The sole source of supply of the apparatus (the Tyler Ro-Tap Sieve Shaker, Model RX-29) known to the committee at this time is W.S. Tyler, Inc., Gastonia, NC. If you are aware of alternative suppliers, please provide this information to ASTM International Headquarters. Your comments will receive careful consideration at a meeting of the responsible technical committee,[1] which you may attend.

[4] The sole source of supply of the apparatus (W.S. Tyler Model 1778-SB) known to the committee at this time is W.S. Tyler, Inc., Gastonia, NC. If you are aware of alternative suppliers, please provide this information to ASTM International Headquarters. Your comments will receive careful consideration at a meeting of the responsible technical committee,[1] which you may attend.

8. Calibration

8.1 Calibration of balances shall be maintained by standard laboratory methods. Sieves shall be calibrated at reasonable intervals in accordance with the procedure described in Specification E11.

9. Procedure

9.1 Determine the nominal particle size of the sample in accordance with Test Method D2862, and its moisture content in accordance with Test Methods D2867.

9.2 Obtain an additional representative sample of approximately 125 mL of the carbon in accordance with Practice E300.

9.3 Screen this sample to its nominal particle size distribution using Test Method D2862. Discard the fractions above the larger and below the smaller nominal particle size. Obtain at least 100 mL of material within the nominal mesh size range. Use additional material obtained as in 9.2, if necessary.

9.4 Measure out 100 mL of the screened sample into a tared, graduated cylinder in accordance with Test Method D2854, and weigh to the nearest 0.1 g.

9.5 Place the hardness pan (Fig. 1) on the standard bottom receiver pan. Pour the screened and weighed sample into the hardness pan and add the steel balls.

9.6 Complete the sieve stack by stacking five full-height sieves and the sieve cover on top of the hardness pan. The extra sieves, in this case, serve only to form a stack which fills the shaker, thus avoiding changes in tapping action and readjustment of the sieve stack retainer.

9.7 Place sieve stack in the sieve shaker and shake for 30 ± 0.5 min, with tapping hammer operating.

9.8 At the end of the shaking period, remove the sieve stack from the sieve shaker and remove the hardness pan from the sieve stack. Place the hardness test sieve on top of the receiving pan.

9.9 Remove the steel balls from the hardness pan and transfer sample to the hardness test sieve, brushing adhering particles into the sieve. Stack the five full-height sieves and sieve cover on top of the hardness test sieve and receiving pan, and replace the stack in the sieve shaker. Shake with the hammer operating for 10 min ± 10 s.

APPENDIX A. STANDARD TEST METHOD FOR BALL-PAN HARDNESS OF ACTIVATED CARBON

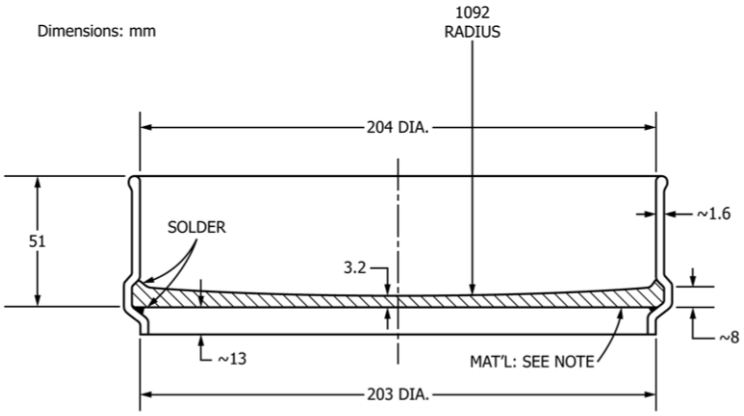

NOTE 1—Material is plate, of one of the following alloys: (*1*) Cartridge brass, UNS C26000, half-hard temper, hardness 60 HRB or greater (see Specification B19); or (*2*) Aluminum bronze, UNS C61400, soft temper, hardness 140 HB or greater (see Specification B150/B150M).

FIG. 1 Pan for Ball-Pan Hardness Test

9.10 At the end of the shaking period, remove the sieve stack from the sieve shaker and transfer the remainder of the sample on the hardness test sieve to a tared weighing pan. Weigh to the nearest 0.1 g.

9.11 Sweep the pan catch into a tared weighing dish, and weigh to the nearest 0.1 g.

10. Calculation

10.1 Calculate the ball-pan hardness number from the equation

$$H = 100\,B/A \quad (1)$$

where:

H = ball-pan hardness number,
B = weight of sample retained on hardness test sieve (see 9.10), g, and
A = weight of sample loaded onto hardness pan (see 9.4), g.

10.2 As a check on the accuracy of the test, calculate ball-pan hardness from the pan catch as follows:

$$H_2 = 100\,(1 - C/A) \quad (2)$$

where:

C = pan catch from 9.11, g.

If H_2 differs from H by more than 2 %, one may assume that significant amounts of carbon are not accounted for, and the run must be rejected.

11. Report

11.1 Report the following information:
11.1.1 Name of the carbon supplier,
11.1.2 Grade designation of the sample,
11.1.3 Nominal particle size range and moisture content (as measured in 9.3),
11.1.4 Ball-pan hardness number,
11.1.5 Name of the agency and technician making the test,
11.1.6 Identification number and date of the test, and
11.1.7 Lot number from which the sample was taken.

12. Precision and Bias[5]

12.1 The precision of this test method is based on an interlaboratory study conducted in 2007. Each of nine laboratories tested four different materials. Every "test result" represents an individual determination. All laboratories submitted three replicate test results (from one operator) for each material.

12.1.1 *Repeatability*—Two test results obtained within one laboratory shall be judged not equivalent if they differ by more than the "*r*" value for that material; "*r*" is the interval representing the critical difference between two test results for the same material, obtained by the same operator using the same equipment on the same day in the same laboratory.

12.1.2 *Reproducibility*—Two test results shall be judged not equivalent if they differ by more than the "*R*" value for that material; "*R*" is the interval representing the difference between two test results for the same material, obtained by different operators using different equipment in different laboratories.

12.1.3 Any judgment in accordance with these two statements would have an approximate 95 % probability of being correct.

12.2 *Bias*—At the time of the study, there was no accepted reference material suitable for determining the bias for this test method, therefore no statement on bias is being made.

12.3 The precision statement was determined through statistical examination of 108 results, from nine laboratories, on four materials. These four carbons are described in Table 2.

[5] Supporting data have been filed at ASTM International Headquarters and may be obtained by requesting Research Report RR:D28-1006.

TABLE 2 Hardness

Carbon	Average	Repeatability Standard Deviation	Reproducibility Standard Deviation	Repeatability Limit	Reproducibility Limit
	$\bar{x}$	*sr*	*sR*	*r*	*R*
Wood 45 sieve	62.37	4.16	16.76	11.66	46.92
Lignite 50 sieve	80.20	1.96	4.46	5.49	12.48
Coconut 16 sieve	99.36	0.18	0.51	0.51	1.44
Bitumi-nous 70 sieve	98.36	0.37	0.73	1.03	2.04

12.4 As noted in the results table, the repeatability and reproducibility are dependent on the carbon type. To judge the equivalency of two test results, it is recommended to choose the carbon closest in characteristics to the test carbon.

Appendix B

Methylene blue adsorption experiments

B.1 Calibration curve

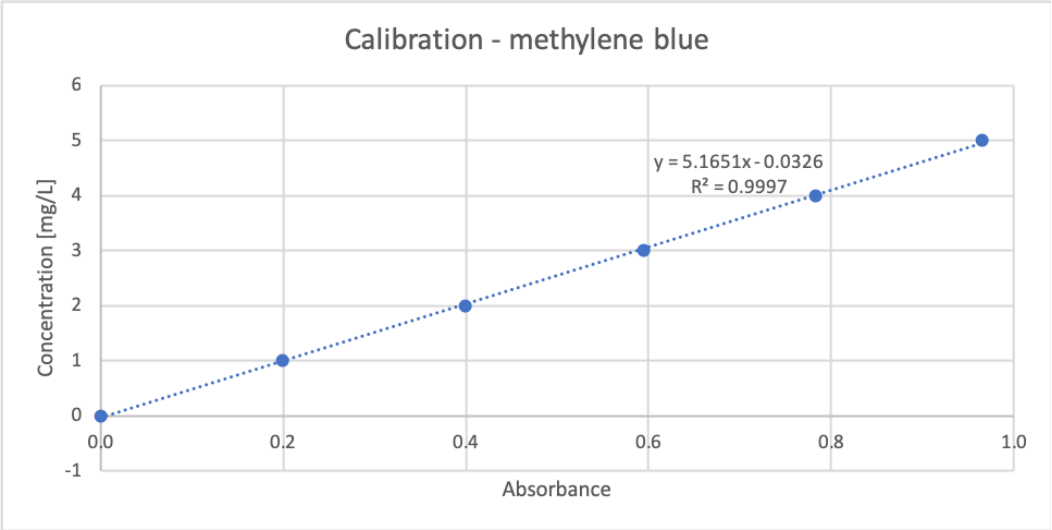

Figure B.1: Calibration curve

B.2 Protocol adsorption isotherm

In the adsorption isotherms tests, 250 mg/L methylene blue solution was prepared with ultrapure water. Different initial amounts of zeolite powders (0, 20, 30, 50, 80, 100, 120, 150, 200, 300, 400, and 500 mg) were added to 100 mL prepared methylene blue solution respectively. Samples (10 mL) were taken after 48 h when the equilibrium was reached. The samples were filtrated through a syringe filter with a 0.45 m polycarbonate membrane and measured with UV spectrophotometer at a maximum wavelength of 665 nm to determine the concentration.

B.3 Freundlich isotherm

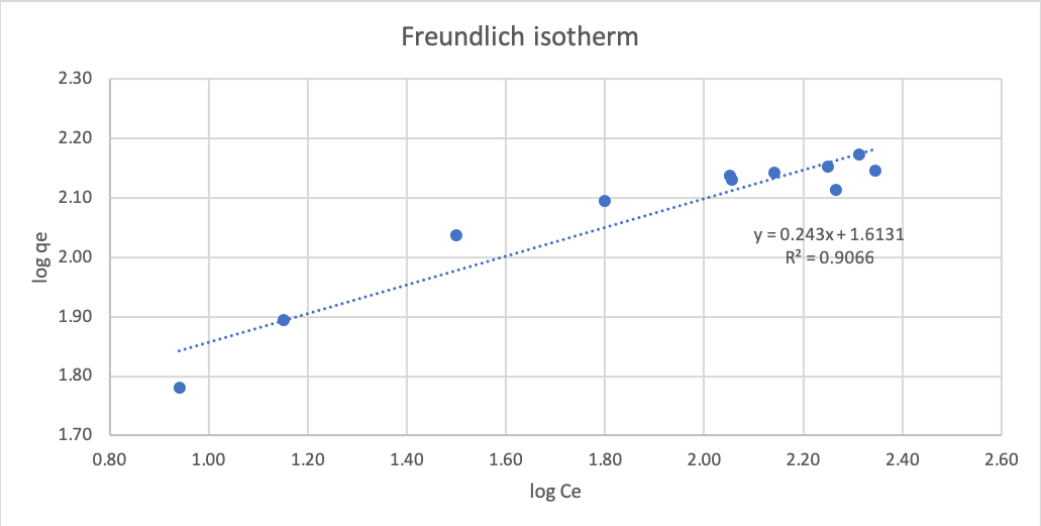

Figure B.2: Freundlich isotherm

Appendix C

Duplicates

C.1 Ball-pan hardness test

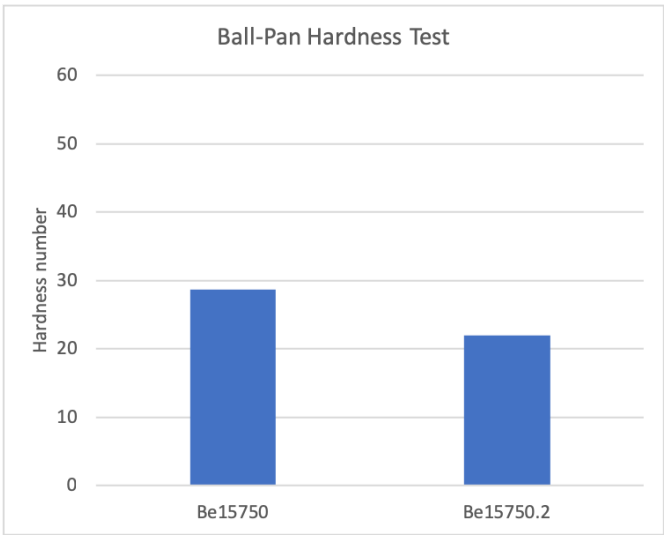

Figure C.1: Ball-pan hardness number: duplicates without polymer

C.2 Mercury intrusion porosimetry

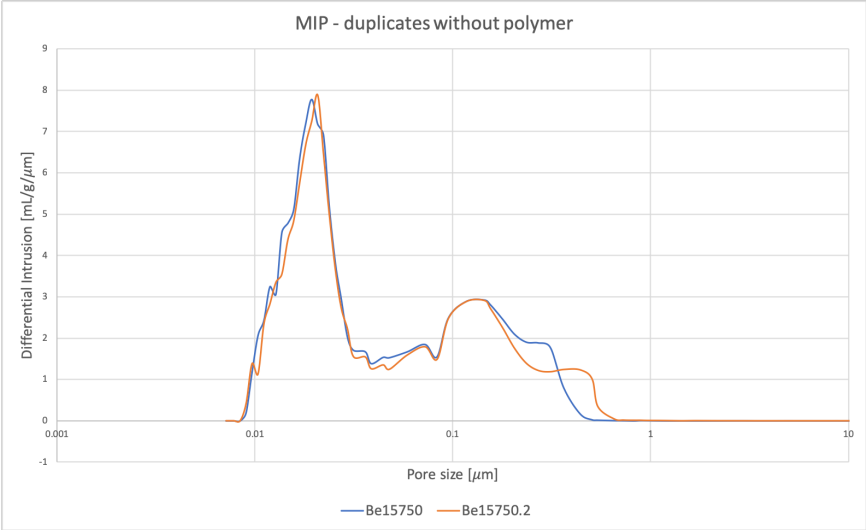

Figure C.2: Mercury intrusion porosimetry: duplicates without polymer

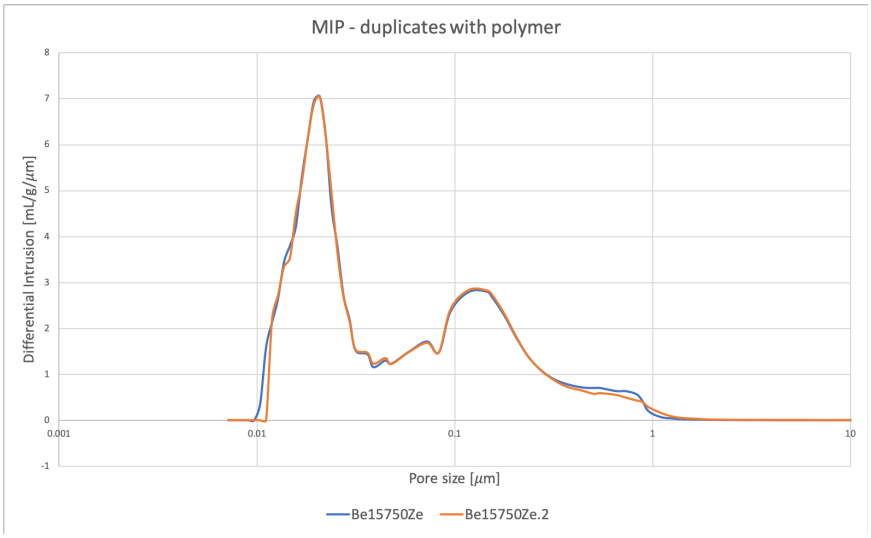

Figure C.3: Mercury intrusion porosimetry: duplicates with polymer

C.3 Methylene blue adsorption

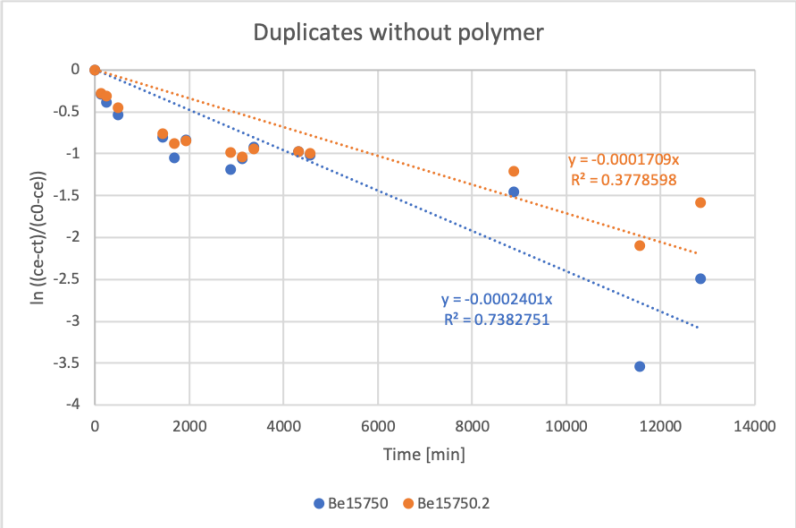

Figure C.4: Methylene blue adsorption: duplicates without polymer

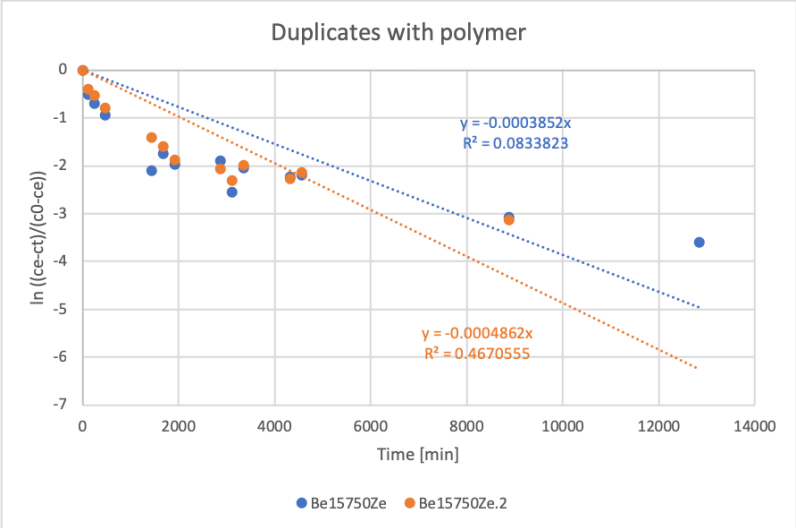

Figure C.5: Methylene blue adsorption: duplicates with polymer

Appendix D

Systems analysis

The influence of the three variable parameters, LDF kinetic rate constant, bulk density and particle density, is analysed individually for the EBCT of 20 and 1 minute. The values of pellet Be15750 are used as the fixed parameters.

D.1 LDF kinetic rate constant

In Figure D.1 and Figure D.2 the kinetic rate constant is varied. A higher kinetic rate leads to a later breakthrough point. The results show that at an EBCT of 20 minutes the kinetic rate constant has little influence on the breakthrough. However, at an EBCT of 1 minute, the kinetic rate constant has a significant effect on the moment of breakthrough.

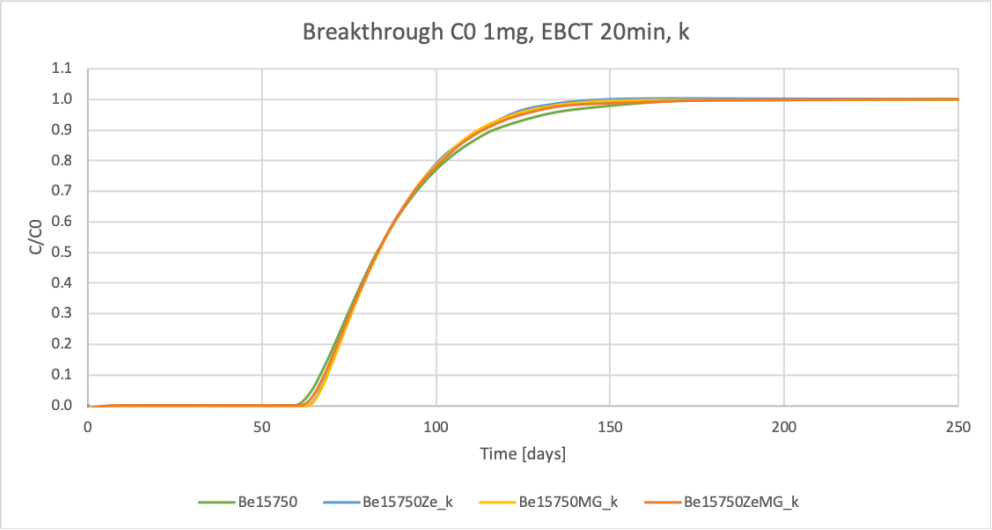

Figure D.1: Breakthrough curves at varying kinetic rate constants. EBCT of 20 minutes.

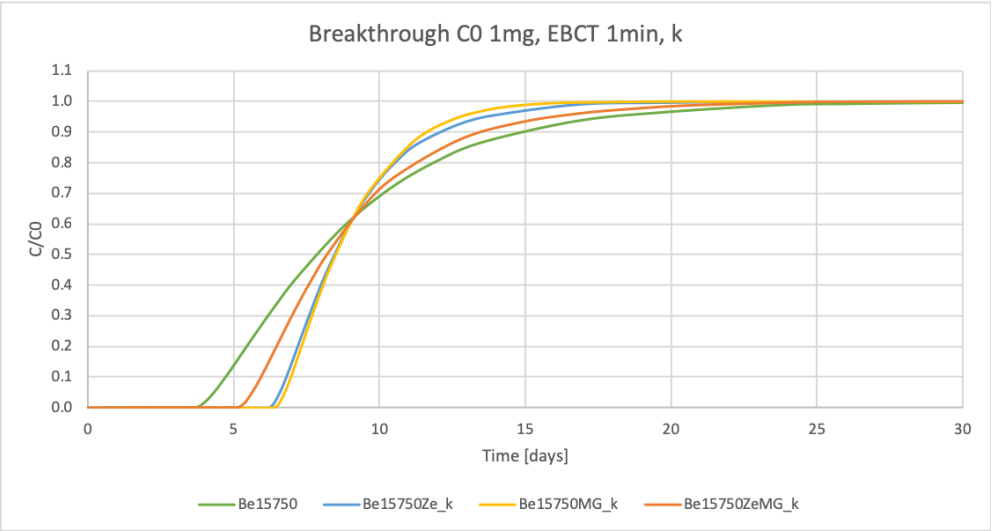

Figure D.2: Breakthrough curves at varying kinetic rate constants. EBCT of 1 minute.

D.2 Bulk density

The bulk density has for both an EBCT of 20 and 1 minute a significant effect on the breakthrough curve (Figure D.3 and Figure D.4). When the bulk density increases, the moment of breakthrough occurs at a later moment for both an EBCT of 20 and 1 minute.

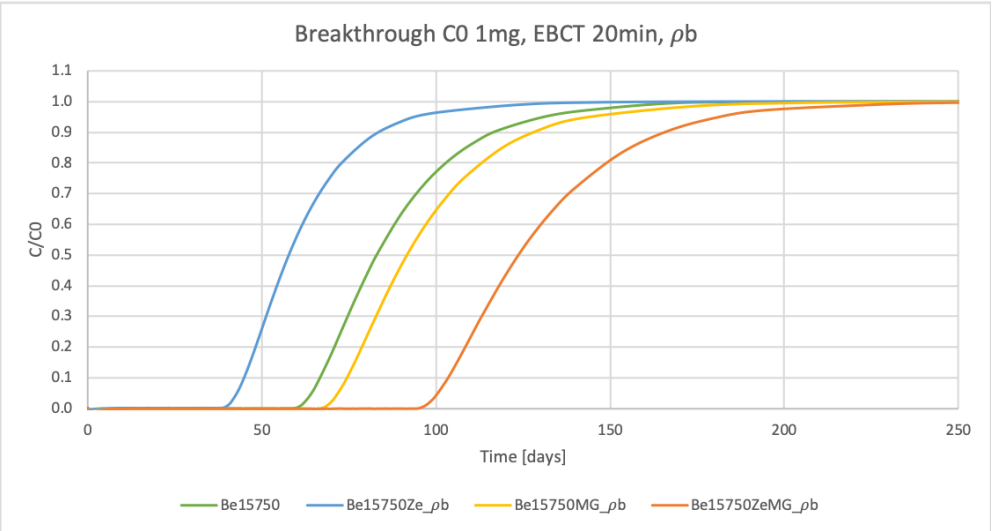

Figure D.3: Breakthrough curves at varying bulk density. EBCT of 20 minutes.

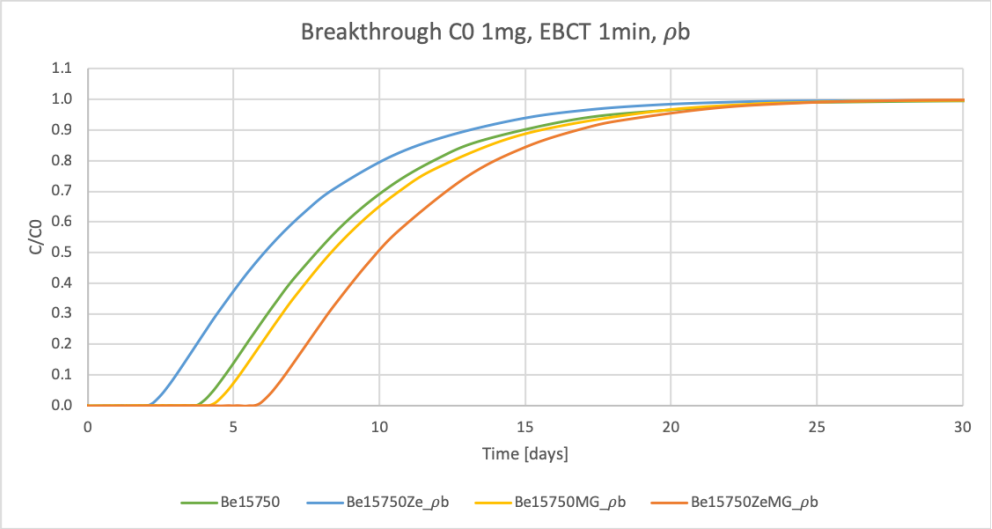

Figure D.4: Breakthrough curves at varying bulk density. EBCT of 1 minute.

D.3 Particle density

When the particle density decreases, the breakthrough point increases for an EBCT of 20 minutes (Figure D.5). However, for an EBCT of 1 minute the particle density has no influence on the breakthrough (Figure D.6).

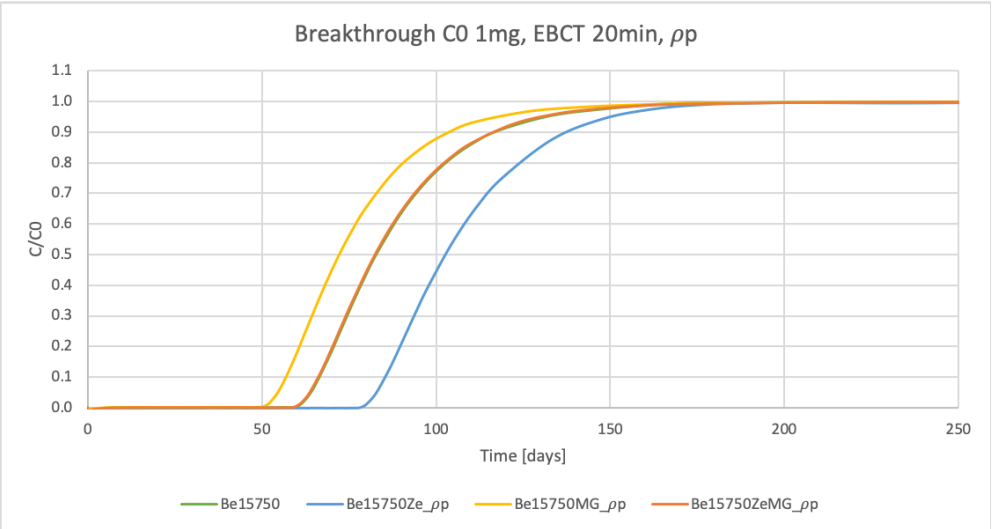

Figure D.5: Breakthrough curves at varying particle density. EBCT of 20 minutes.

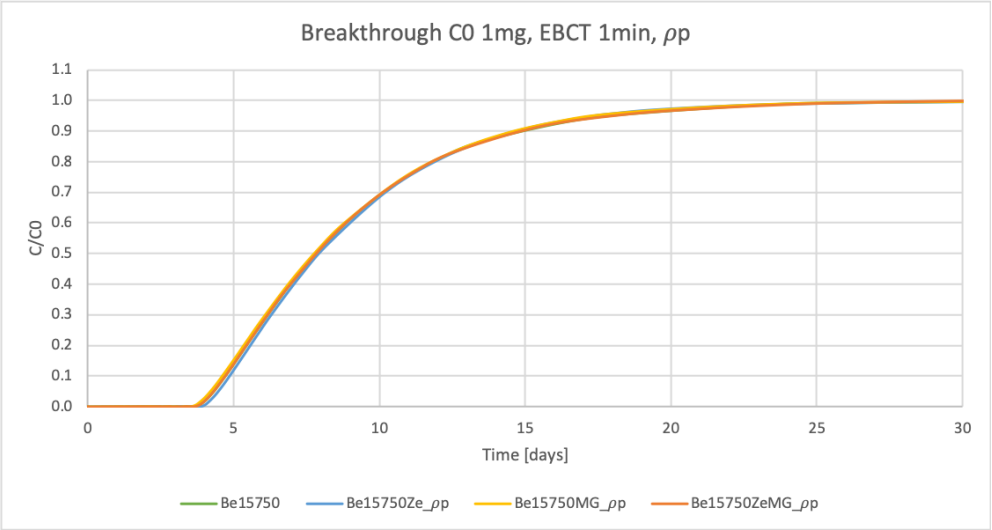

Figure D.6: Breakthrough curves at varying particle density. EBCT of 1 minute.